NSTAR Extended Life Test Discharge Chamber Flake Analyses

Kim K. de Groh and Bruce A. Banks
Glenn Research Center, Cleveland, Ohio

Christina A. Karniotis
QSS Group, Inc., Cleveland, Ohio

March 2005

The NASA STI Program Office . . . in Profile

Since its founding, NASA has been dedicated to the advancement of aeronautics and space science. The NASA Scientific and Technical Information (STI) Program Office plays a key part in helping NASA maintain this important role.

The NASA STI Program Office is operated by Langley Research Center, the Lead Center for NASA's scientific and technical information. The NASA STI Program Office provides access to the NASA STI Database, the largest collection of aeronautical and space science STI in the world. The Program Office is also NASA's institutional mechanism for disseminating the results of its research and development activities. These results are published by NASA in the NASA STI Report Series, which includes the following report types:

- TECHNICAL PUBLICATION. Reports of completed research or a major significant phase of research that present the results of NASA programs and include extensive data or theoretical analysis. Includes compilations of significant scientific and technical data and information deemed to be of continuing reference value. NASA's counterpart of peer-reviewed formal professional papers but has less stringent limitations on manuscript length and extent of graphic presentations.

- TECHNICAL MEMORANDUM. Scientific and technical findings that are preliminary or of specialized interest, e.g., quick release reports, working papers, and bibliographies that contain minimal annotation. Does not contain extensive analysis.

- CONTRACTOR REPORT. Scientific and technical findings by NASA-sponsored contractors and grantees.

- CONFERENCE PUBLICATION. Collected papers from scientific and technical conferences, symposia, seminars, or other meetings sponsored or cosponsored by NASA.

- SPECIAL PUBLICATION. Scientific, technical, or historical information from NASA programs, projects, and missions, often concerned with subjects having substantial public interest.

- TECHNICAL TRANSLATION. English-language translations of foreign scientific and technical material pertinent to NASA's mission.

Specialized services that complement the STI Program Office's diverse offerings include creating custom thesauri, building customized databases, organizing and publishing research results . . . even providing videos.

For more information about the NASA STI Program Office, see the following:

- Access the NASA STI Program Home Page at *http://www.sti.nasa.gov*

- E-mail your question via the Internet to help@sti.nasa.gov

- Fax your question to the NASA Access Help Desk at 301–621–0134

- Telephone the NASA Access Help Desk at 301–621–0390

- Write to:
  NASA Access Help Desk
  NASA Center for AeroSpace Information
  7121 Standard Drive
  Hanover, MD 21076

NSTAR Extended Life Test Discharge Chamber Flake Analyses

Kim K. de Groh and Bruce A. Banks
Glenn Research Center, Cleveland, Ohio

Christina A. Karniotis
QSS Group, Inc., Cleveland, Ohio

National Aeronautics and
Space Administration

Glenn Research Center

March 2005

Acknowledgments

NSTAR Extended Life Test Discharge Chamber Flake Analyses

Kim K. de Groh and Bruce A. Banks
National Aeronautics and Space Administration
Glenn Research Center
Cleveland, Ohio 44135

Christina A. Karniotis
QSS Group, Inc.
Cleveland, Ohio 44135

Summary

The Extended Life Test (ELT) of the NASA Solar Electric Propulsion Technology Readiness (NSTAR) ion thruster was concluded after 30,352 hours of operation. The ELT was conducted using the Deep Space 1 (DS1) back-up flight engine, a 30 cm diameter xenon ion thruster. Post-test inspection of the ELT engine revealed numerous contaminant flakes distributed over the bottom of the cylindrical section of the anode within the discharge chamber (DC). Extensive analyses were conducted to determine the source of the particles, which is critical to the understanding of degradation mechanisms of long life ion thruster operation. Analyses included: optical microscopy (OM) and particle length histograms, field emission scanning electron microscopy (FESEM) combined with energy dispersive spectroscopy (EDS), and atomic oxygen plasma exposure tests. Analyses of the particles indicate that the majority of the DC flakes consist of a layered structure, typically with either two or three layers. The flakes comprising two layers were typically found to have a molybdenum-rich (Mo-rich) layer on one side and a carbon-rich (C-rich) layer on the other side. The flakes comprising three layers were found to be sandwich-like structures with Mo-rich exterior layers and a C-rich interior layer. The presence of the C-rich layers indicates that these particles were produced by sputter deposition build-up on a surface external to the discharge chamber from ion sputter erosion of the graphite target in the test chamber. This contaminant layer became thick enough that particles spalled off, and then were electro-statically attracted into the ion thruster interior, where they were coated with Mo from internal sputter erosion of the screen grid and cathode components. Atomic oxygen tests provided evidence that the DC chamber flakes are composed of a significant fraction of carbon. Particle size histograms further indicated that the source of the particles was spalling of carbon flakes from downstream surfaces. Analyses of flakes taken from the downstream surface of the accelerator grid provided additional supportive information. The production of the downstream carbon flakes, and hence the potential problems associated with the flake particles in the ELT ion thruster engine is a facility induced effect and would not occur in the space environment.

Nomenclature

A	total area of flakes, cm^2
M_T	total mass of the flakes prior to ashing, g
M_T'	total mass of flakes after ashing, g
ρ_{Mo}	density of Mo, g/cm^3
ρ_C	density of C, g/cm^3
X_C	average thickness of C layer, μm
X_{Mo}	average thickness of Mo layer, μm
X_T	total thickness of flake prior to ashing, μm

I. Introduction

NASA's Deep Space 1 (DS1) spacecraft provided the first successful flight of an ion propulsion system.[1] The DS1 mission was launched in October of 1998 and included a July 1999 flyby of the Asteroid Braille and a September 2001 encounter of the Comet Borelly. DS1 was a technology validation mission, flying a single 30-cm-diameter xenon ion engine, provided by the NASA Solar Electric Propulsion Technology Readiness (NSTAR) project, as its primary propulsion system. The ion thruster successfully completed the mission in December of 2001, processing in excess of 73 kg of propellant and accumulating 16,265 hours of operation in space.[2] Details on the DS1 ion thruster mission performance can be found in references 3 to 5. The mission was a success, stimulating future NASA science missions utilizing solar electric propulsion to demand lifetimes and propellant throughput in excess of 20,000 hours and 200 kg.[2] As a result, assessing the ultimate service life capability of the technology is vital, requiring extensive ground testing and data analysis.[2]

A long duration test, called the Extended Life Test (ELT) of the Deep Space 1 (DS1) spare flight ion thruster (FT2) has been conducted at the Jet Propulsion Laboratory (JPL) in collaboration with the NASA Glenn Research Center (GRC). The ELT was started in October 1998 and was concluded on June 26, 2003. The ELT was voluntarily terminated prior to its end of life so that analyses of the engine components could be conducted to provide critical information for ion propulsion system designers working on engines for near-term NASA missions. The primary purpose of the ELT was to determine the ultimate service life capability of the NASA 30-cm ion thruster technology. During its 5-year run, the thruster operated for a total of 30,352 hours and processed 235 kg of xenon propellant.[6] The objectives of the test were to characterize known failure modes, identify unknown failure modes, and to measure performance degradation with thruster wear.[2] Thruster performance data and operational characteristics, over the full DS1 throttle range, were collected and analyzed extensively during the course of the test. Review of the performance of the ELT can be found in references 2 and 6 to 8. Figure 1 is a photograph of the DS1 FT2 taken shortly after completion of the ELT. Extensive post-test inspection and analyses have been conducted at JPL and at the NASA GRC with collaborative efforts from other groups. Results from these studies can be found in references 6, 7, 9, and 10.
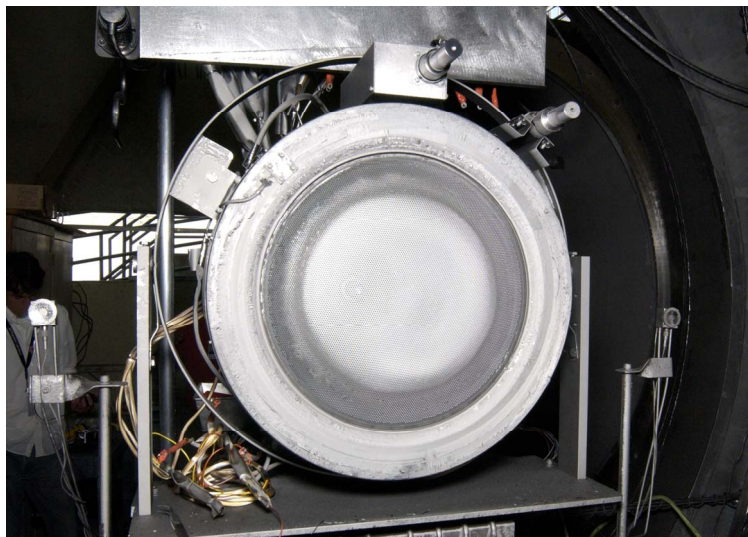

Figure 1. NSTAR ELT Ion Thruster after 30,352 hours of operation.

Post-test inspection of the ELT engine revealed numerous small contaminant flakes uniformly distributed over the bottom of the cylindrical section of the discharge chamber (DC), as shown in Figure 2. Flakes were not observed on the conical area of the DC. The presence of these flakes was unexpected. Internally generated flakes are a major threat to thruster reliability and durability because they can potentially short the ion optics or the cathode. If the flakes are externally generated (from the facility) then these flakes are not a threat to in-space reliability and durability. Therefore, it is important to determine the origin of the flakes, which is critical to the understanding of degradation mechanisms of long life ion thruster operation. The contaminant flakes were therefore collected for evaluation.
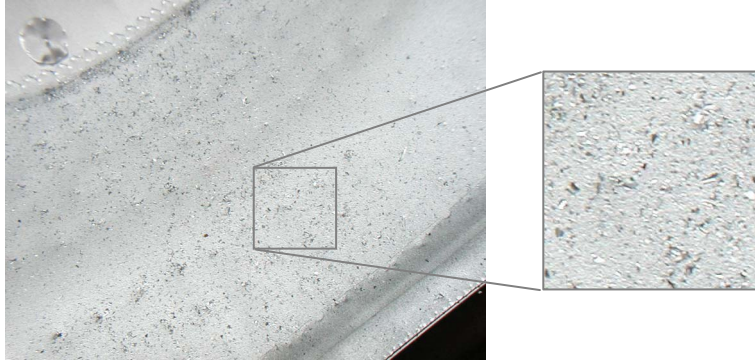
Figure 2. Contaminant flakes distributed over the bottom of cylindrical section of the NSTAR DC.

Extensive analyses have been conducted at the GRC on NSTAR ELT DC contaminant flakes to determine the source of the particles (e.g. from within the thruster, from the screen or accelerator grids, or from outside the thruster). Analyses included particle shape and size, surface and edge texture and chemistry, and edge thickness. A particle size histogram was produced. Atomic oxygen exposure tests were conducted on a group of flakes to determine the quantity of carbon present. Samples were collected of loose downstream accelerator grid surface sputter deposited debris. The loose downstream accelerator grid and ground shield surface debris is shown in Figure 3. This photograph was taken at the perimeter of the downstream surface accelerator grid. The downstream accelerator grid debris was analyzed for its composition to provide additional information for verifying the source of DC contaminant flakes. Samples of the anode screen mesh were sectioned and examined for evidence of deposited coating spalling. This paper summarizes the results of the analyses of the DC flakes, the downstream accelerator grid debris and the sputter containment mesh, providing evidence for the source of the particles.
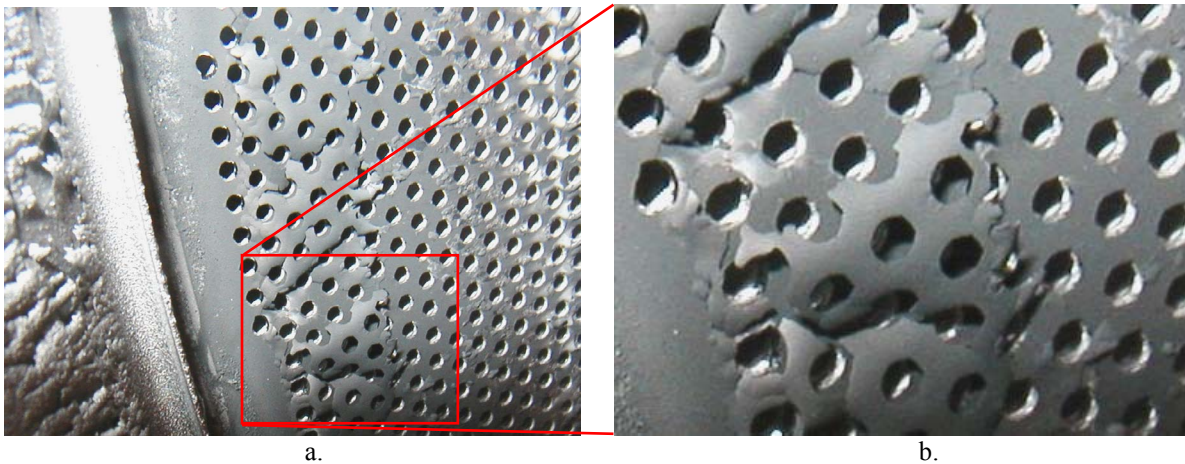

a.   b.

Figure 3. Loose sputter deposited debris on the downstream accelerator grid: a). Perimeter of grid, and b). close-up image of debris shown in a).

II.   Experimental Procedures

A. Materials
1. Discharge Chamber (DC) Flakes
The NSTAR DC flakes were swept into 18 visually equal sized "zones" using trimmed down acid brushes and then collected and put into 18 containers. The remaining very small flakes were swept into a "No #" container. JPL supplied GRC with containers labeled: DC Flakes 3, DC Flakes 14, DC Flakes 15, DC Flakes 16, DC Flakes 17, and DC Flakes (No #). The remaining containers remained at JPL.

2. Accelerator Grid Downstream Surface Flakes

Loose flake particles were collected from the downstream accelerator grid surface. These relatively large flakes were in the process of spalling off the surface, as shown in Figure 2, and were easily lifted off. Pieces of the downstream accelerator grid flake pieces were mounted on the SEM holder propped up at angles so that the edges of the flakes were visible for imaging and EDS analyses.

3. Sputter Containment Anode Mesh Samples

GRC was provided with two sets of six containment mesh samples sectioned from the anode. The anode mesh samples were sectioned in axial "sets." These sets were sectioned in radially equal positions from within the DC, so that each set was obtained in a line with the first sample being cut closest to the cathode and the last sample being cut closest to the grids. One set of samples provided to GRC contained Anode Mesh Samples 21-26. Samples 21-23 were located in the conical portion of the thruster with Sample 21 being closest to the cathode. Samples 24-26 were located in the cylindrical portion of the thruster with Sample 26 being closest to the screen grid. These samples were sectioned with approximately equal distances between each sample. The second set of samples contained Anode Mesh Samples 3-5 and 30-32. Samples 3-5 were from the conical portion of the thruster with 3 being closest to the cathode, and Samples 30-32 were from the cylindrical portion of the thruster with 32 being closest to the screen grid.

Two sputter containment mesh samples (Sample 21 and 26) were sent to the University of Dayton Research Institute for analysis. These samples were cross-sectioned and potted, then analyzed using SEM and EDS at 25 kV to determine the composition of the coating.

B. Optical Microscopy

Optical micrographs of the DC and accelerator grid flakes were taken using an Olympus SZH Stereo-zoom microscope outfitted with a Canon D30 digital camera. The four original containers of DC flakes were divided into quadrants and numerous low magnification images (12.5 X) of each of the quadrants were taken to document the size and shape of the majority of flakes.

The optical microscopy images of flakes from containers DC Flakes 15 and 17 were used to create a size distribution chart. The longest dimension of 1538 flakes was measured (645 flake measurements from DC 15 and 893 flake measurements from DC Flake 17) and the flakes were grouped into 0.1 mm size bins. The results were used to create a particle size histogram showing size distribution as a function of the number of particles.

C. Field Emission Scanning Electron Microscopy (FESEM) and Energy Dispersive Spectroscopy (EDS)

Scanning electron microscope images were obtained using a Hitachi S-4700 FESEM operated at 6 kV and 25 kV. Because of the interest in conducting analytical analyses, flake particles were imaged without applying conductive films; therefore, the lower energy accelerating voltage of 6 kV was typically used for analyses. Four batches of flakes, identified as B1 through B4, were mounted on four holders using either silver paint or double stick carbon conductive tape. Energy dispersive spectroscopy was conducted using an EDAX CDU Leap Detector system and standard-less semi-quantitative data was obtained from the spectra.

D. Atomic Oxygen Exposure for Mass Loss Analysis

Atomic oxygen was used to conduct a mass loss analysis to determine the approximate amount of carbon in the flakes versus the non-organic material. A group of flakes were weighed on a cleaned fused-silica slide prior to, and after, atomic oxygen exposure using a Mettler M3 Analytical Balance. The fused silica slide was pre-cleaned by exposing it to atomic oxygen in a RF (radio frequency) plasma asher operated on air for 120 hours to remove any oils or residue present. The flakes and cleaned slide were exposed to atomic oxygen in the asher for 115 hours. The mass loss of the flakes theoretically corresponds to the amount of carbon present in the flakes before ashing.

III.   Results and Discussion

In ground-laboratory ion thruster tests ion sputter erosion will take place within the vacuum facility downstream of the thruster. Therefore, a low sputter yield material, such as carbon (C) in the form of graphite or Grafoil, is

placed inside the vacuum tank downstream of the engine covering the view of the facility tank material (stainless steel), which has a higher sputter yield. This low sputter erosion material is typically called the target. The sputter eroded target material will deposit and coat downstream surfaces of the thruster, and can also enter into the DC, as shown in Figure 4. In the ELT the target material was carbon in the form of graphite panels. During ion thruster operation, both in-space and during ground tests, significant sputter erosion of thruster components also occurs. In particular, the xenon ions sputter erode the up-stream surfaces of the screen grid, and the hole walls and downstream surfaces of the accelerator grid. The grids are comprised of molybdenum (Mo) in the NSTAR engine. The screen grid and (to a lesser extent) accelerator grid hole wall sputter eroded Mo can deposit on the inside of the DC and a thick layer of sputter deposited Mo builds up within the DC during a long-duration test. Therefore, the DC is lined with a sputter containment mesh comprised of a high surface area (grit-blasted) woven stainless steel mesh. The containment mesh was designed to retain the sputter deposited Mo. The high surface area minimizes the stresses that build up as the film gets thick and hence resists spalling of the deposited film. Other sources of sputter deposition inside the DC are from cathode components (the keeper tube comprised of tantalum (Ta), the keeper end cap (Mo), or the cathode orifice plate (thoriated tungsten (W)), also shown in Figure 4.
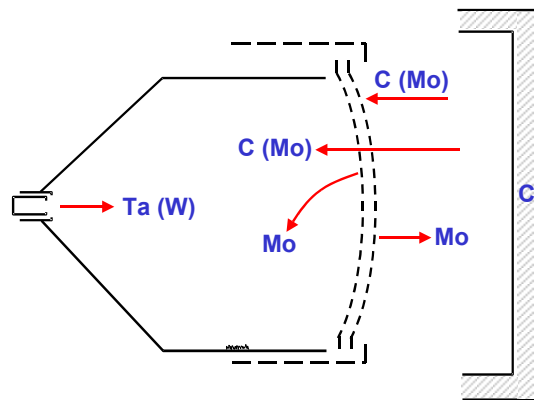

Figure 4. Schematic drawing showing the primary modes of ion sputter erosion and deposition occurring during the NSTAR ELT thruster test.

As the ion sputter erosion and deposition processes take place, numerous possibilities exist for building up a thick enough film deposit that can then spall and become a source of contaminant flakes in the ELT ion thruster DC. The most probable source locations for contaminant flakes found in the ion thruster are provided in Figure 5. These include: 1. the cathode keeper area, 2. the anode mesh, 3. the perimeter of the upstream face of the screen grid, 4. the screen grid hole walls, 5. the accelerator grid hole walls, 6. the perimeter of the downstream face of the accelerator grid, and 7. the downstream face of the thruster ground shield. By examining the shape and chemistry of the DC flakes and comparing the results with flakes taken from the downstream accelerator grid surface, and examining the sputter containment mesh, the source of the ELT DC flakes can be determined.
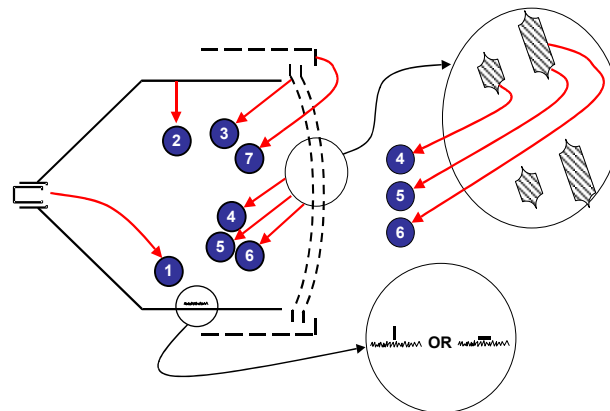

Figure 5. Schematic drawing showing the potential source locations of the contaminant flakes that deposited in the NSTAR ELT DC.

A. Discharge Chamber (DC) Flakes

1. Optical Microscopy

The optical microscopy images of the DC flakes clearly show that there are differences in the appearance of the individual flakes. The flakes differ in color (light, medium and dark) and texture (relatively smooth and shiny or rough), as seen in Figure 6. The shiny flakes have a metallic appearance. This heterogeneity in flake appearance is most likely due to a difference in surface chemistry and corresponding texture. Looking more closely at certain flakes it was observed that some showed differences in color and texture on the same flake. Examples of this type of dual-texture flake are provided in Figure 7.
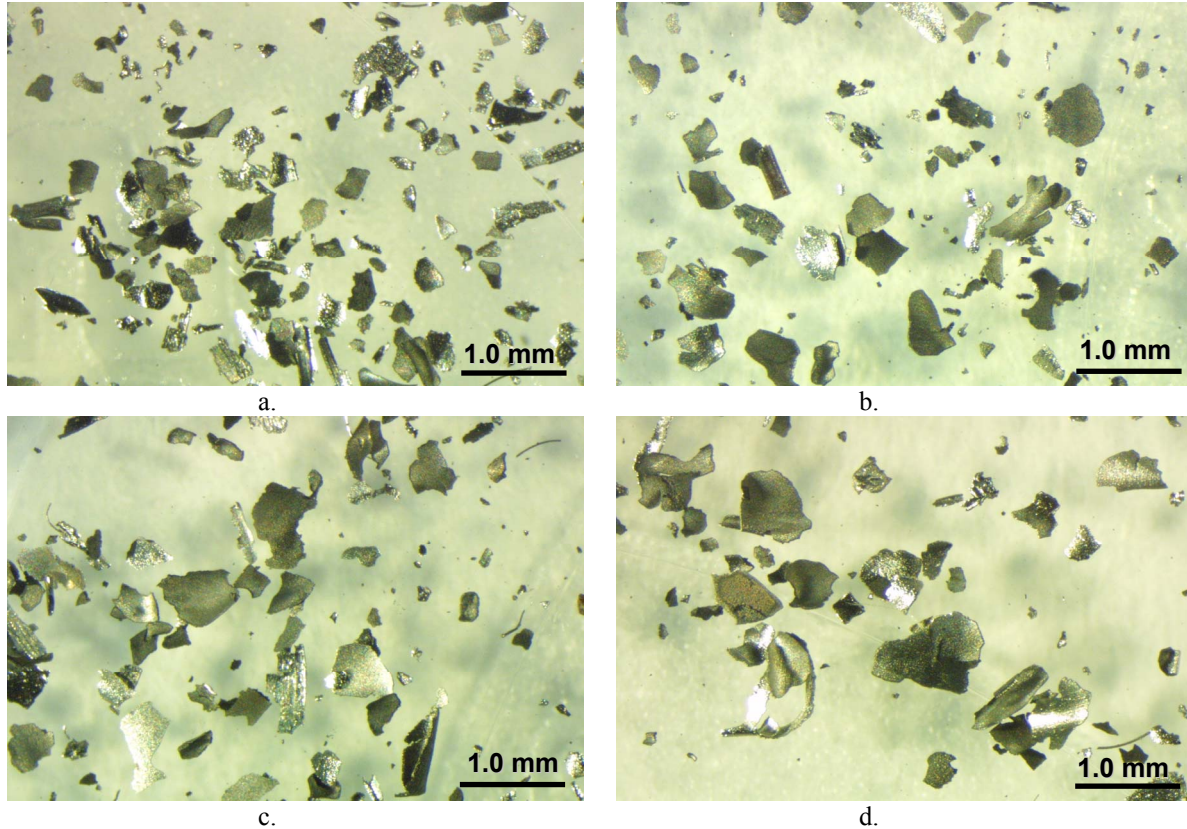

Figure 6. Optical micrograph images of the DC flakes showing contrasting textures and hues of flakes: a). Image 4260 from DC Flakes 16, b). Image 4239 from DC Flakes 16, c). Image 4300 from Flakes 16 and d). Image 4388 from DC Flakes 17.
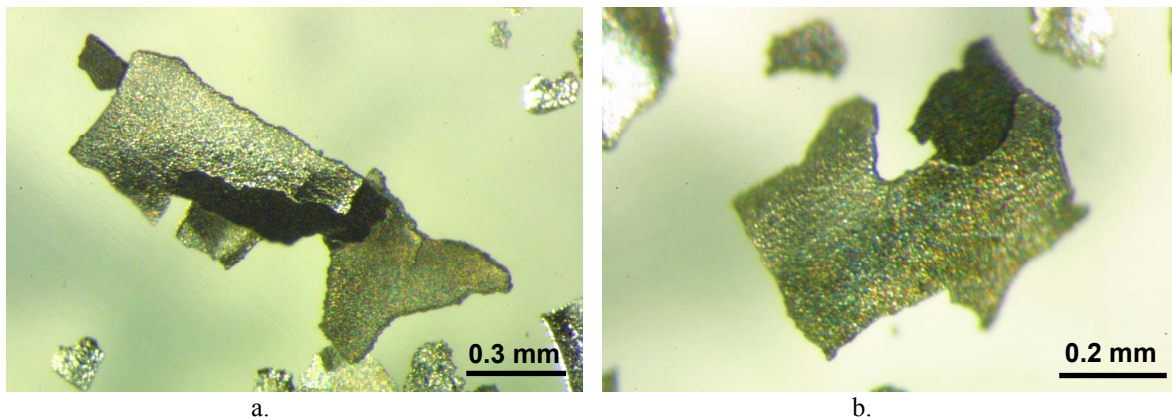

Figure 7. Optical micrograph images of dual-texture flakes showing contrasting textures and hues on single flakes: a). Image 4424 from DC Flakes 16, and b). Image 4459 from DC Flakes 16.

The optical microscope images revealed at least four flakes whose shape suggested that they had spalled from the area around either the screen or accelerator grid holes (i.e. the flakes resided within the grid hole wall). The theoretical diameter of the grid hole from which these flakes may have originated was determined by fitting a circle of a known diameter into the arc of the flakes. An example is provided in Figure 8. Three of the four flakes measured were found to correspond to the post-test accelerator hole diameters, while one is somewhat larger. This is not surprising as it is very likely that because these flakes are under compressive stresses when deposited, they may expand somewhat as they spall and lift off the surface. None of the flakes indicated that they were from the larger screen grid hole wall.

Figure 8. NSTAR DC flake that appears to have resided within a hole wall (Image 4242, DC Flakes 15).

The particle size histogram created from the flake measurements is provided in Figure 9. This histogram shows that a large majority of the flakes are smaller than 0.5 mm in length. As can be seen in the histogram, as the flake size increases the number of flakes decreases. At a length of 0.8 mm and above, less than 10 flakes appeared in each 0.1 mm increment bin. Thirteen flakes were measured to be ≥1.0 mm in length that were included in the histogram. It should be noted that not all of the flakes in the DC Flakes 17 container were measured, and none of the DC Flakes 3, 14 or 16 were measured for the histogram, therefore this is a general representation of the flake sizes.

The two largest flakes included in the histogram were 1.403 and 1.430 mm in length. The 1.403 mm flake is shown in Figure 10 below with a 1.189 mm length flake (B2 P10). These flakes, along with all the histogram flakes are consistent with being of a size that could fit through the accelerator grid holes. The histogram therefore indicates that the size of the DC flakes was controlled by the grid hole sizes, with the accelerator grid holes acting like a filter. This indicates that the flakes originated outside the DC. If the flakes had originated from spalling of material on the screen anode, inside the DC, then much longer flakes would have been observed.

The number of flakes included in the histogram that are larger than the post-test grid gap and therefore could bridge the gap between the grids is 160. Therefore, based on the histogram data, 10.4% of the flakes could cause a short between the grids.
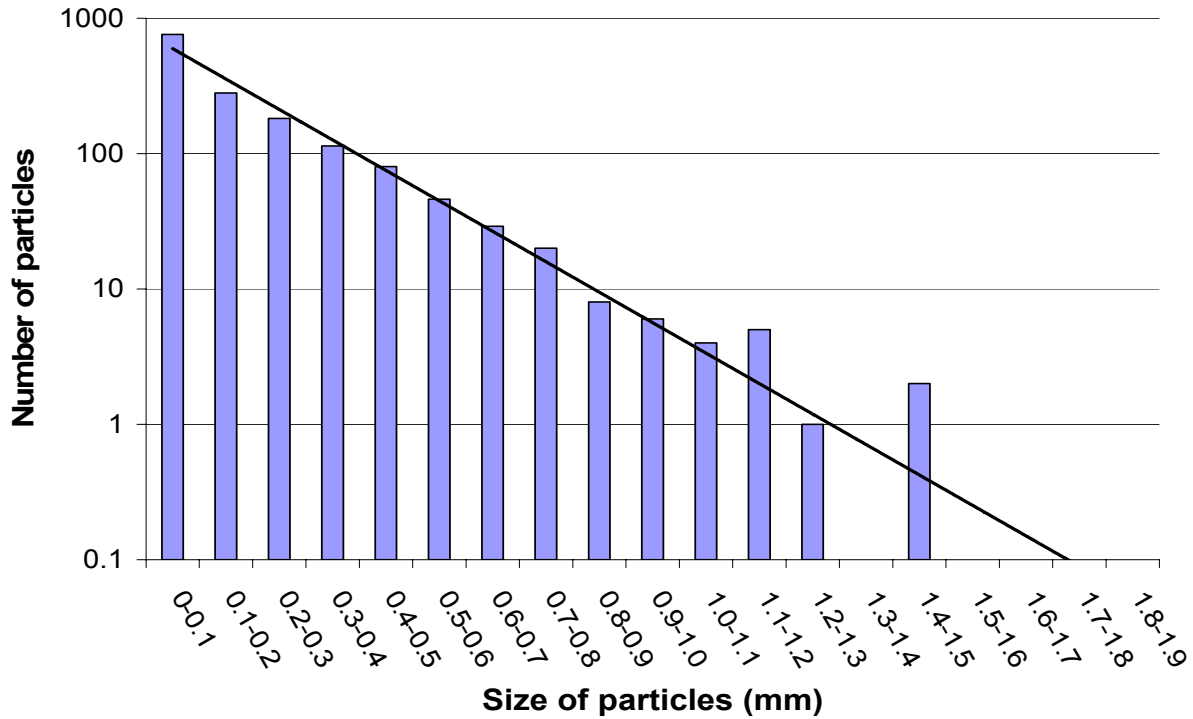
Figure 9. Particle size histogram based on the longest dimension of 1538 flakes (645 from DC Flakes 15 and 893 from DC Flakes 17).
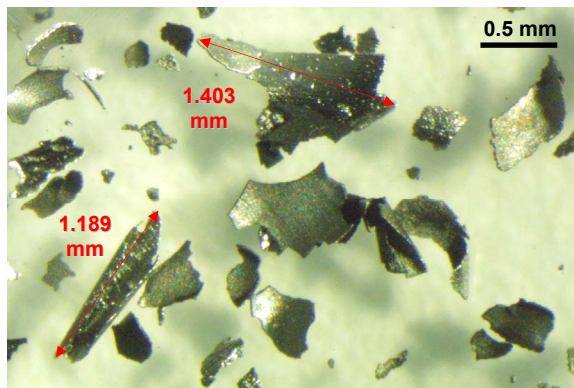

Figure 10. Optical microscope image showing two of the largest measured flakes (Image 4445, DC Flakes 17).

2. EDS Data Information

The detector on the FESEM EDS system is very sensitive to light elements, hence low energy peaks. It was discovered that there is a very large peak at 0.18 keV that is present in Mo-rich spectra obtained at 6 keV using the EDAX CDU Leap Detector for this research. This coincidentally is at the same peak position for boron. A small 0.18 keV peak was present in the 25 kV spectrums. Analyses were conducted to determine the identity of this peak. EDS spectra for a Mo standard were obtained at 6 kV and 25 kV, and are provided in Figure 11a and 11b, respectively. Both of these spectra have the 0.18 keV peak along with the Mo M lines at 2.29 and 2.39 keV and an oxygen peak. Therefore, it is evident that the 0.18 keV peak is characteristic of the Mo spectra as obtained with this detector.
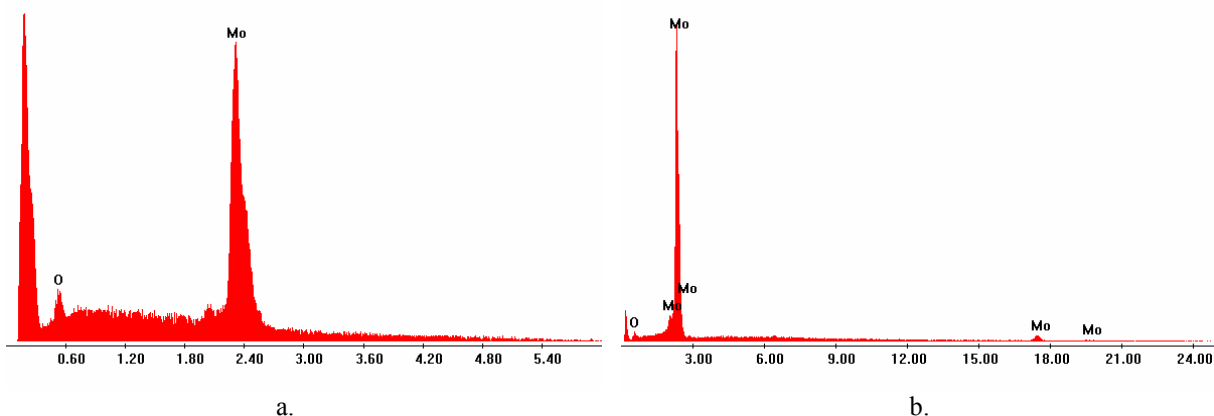
Figure 11. EDS spectra for a Mo standard: a). At 6 kV (12-9-03 S1), and b). At 25 kV (12-9-03 S6).

A section of a spare Mo grid was also analyzed using the EDAX CDU Leap Detector system at 6 and 25 keV. It was desired to verify the presence of the 0.18 keV Mo peak with the Mo grid material and to identify any other elements that may be present in the grid spectra. This also allowed for direct comparisons between the DC flake spectra and the Mo grid spectra by utilizing a multiple spectrum display feature in the EDS software. The sample was cut from the grid such that a fractured section of material was analyzed and the corresponding EDS spectra obtained at 6 kV and 25 kV are provided in Figures 12a and 12b, respectively. The 6 kV spectrum is very similar to the Mo standard spectrum at 6 kV, with a large peak at 0.18 keV (this peak is smaller in the grid spectrum than in the standard spectrum). The 25 kV spectrum is also similar to the Mo standard, but has a small peak identified as aluminum (Al) that is not present in the Mo standard spectrum at 25 kV.
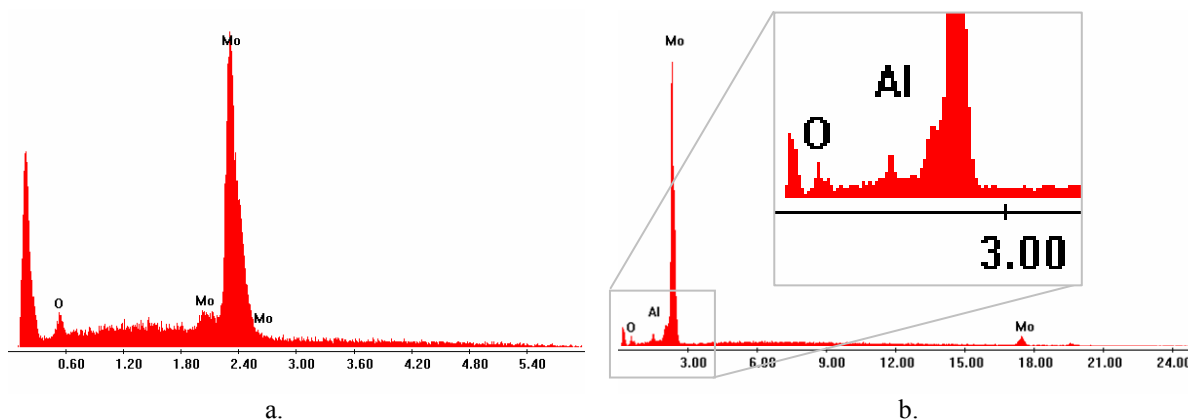

Figure 12. EDS spectra of the Mo grid sample: a). At 6 kV (3-2-04 S1), and b). At 25 kV (3-2-04 S2).

Figure 13 provides an EDS spectrum for a Mo-rich DC flake obtained at 6 kV along with various Mo lines highlighted through the EDS software. The 2 tall blue lines indicate two Mo L lines at 2.29 keV ($L_{III}M_V$) and 2.39 keV ($L_{II}M_{IV}$). The yellow line indicates a Mo M line at 0.35 keV ($M_{II}N_I$). This sits at the same peak position as nitrogen. The Mo M line that resides at 0.18 keV ($M_{II}M_{IV}$) is not identified in this EDS software program.

One of the complications with the large 0.18 keV peak is that it is so close to the primary C $K\alpha_1$ peak (0.277 keV) that quantitative C percentages can be very inaccurately identified. For example, if C is listed as one of the elements to quantify (along with Mo and O) in the Mo standard spectrum, the software computes the presence of 41 atomic percent (AT%) C. Figure 14 shows the peak fits used (light blue line) for the Mo standard spectrum (in red) and the corresponding percentages identified when the quantification program is run. The overlap of C onto the 0.18 keV Mo line is shown in this figure.
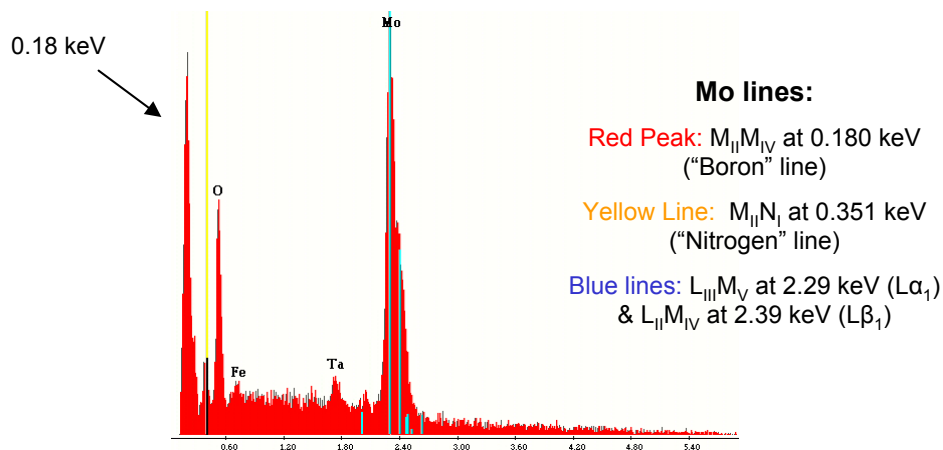
Figure 13. EDS spectrum for a Mo rich DC flake at 6 kV with the various Mo line peaks identified.
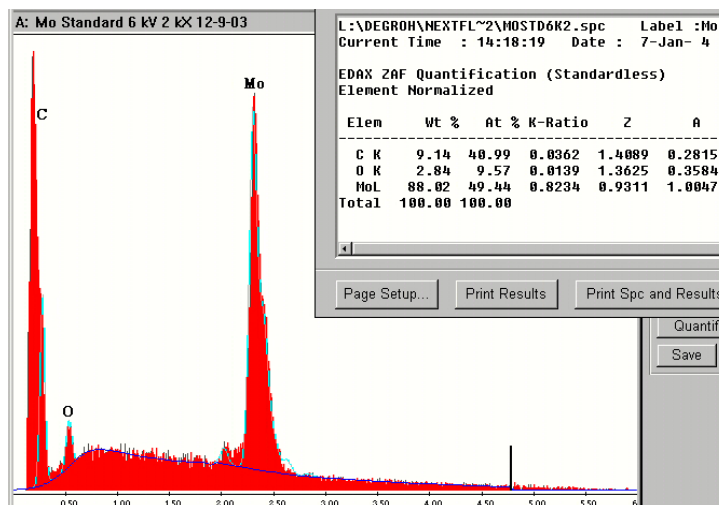

Figure 14. EDS quantification software curve fits including C for a Mo standard spectra at 6 kV.

Semi-quantitative data for the Mo standard and the Mo grid spectra, at 6 kV and 25 kV, are provided in Tables 1 and 2, respectively. The data has been computed both with and without C identified. At 6 kV the Mo grid has 88.1 AT% Mo and 11.9 AT% O. An Al peak is not clearly present, but 1.7 AT% Al is indicated when identified. If C is identified, then at 6 kV the grid is identified as having 70.9 AT% Mo, 19.9 AT% C and 9.4 AT% O, and at 25 kV, the grid is identified as having 48.8 AT% Mo, 36.5 AT% C, 13.2 AT% O and 1.4 AT% Al. So, although the 0.18 keV peak is smaller in comparison to the 2.29 keV Mo peak at 25 kV, the quantity of "C" is larger. The 6 kV EDS data are used rather than the 25 kV data, when available throughout this report.

Table 1. Semi-Quantitative Data for a Mo Standard at 6 kV and 25 kV.

Mo Std 6 kV			Mo Std 25 kV		
Element	Wt %	At %	Element	Wt %	At %
Mo	96.8	83.3	Mo	92.8	68.2
O	3.2	16.7	O	7.2	31.8
Mo Std 6 kV with "C"			Mo Std 25 kV with "C"		
Element	Wt %	At %	Element	Wt %	At %
Mo	88.0	49.4	Mo	83.7	41.6
C	9.1	41.0	C	10.0	39.7
O	2.8	9.6	O	6.3	18.7

Table 2. Semi-Quantitative Data for a Mo Grid Sample at 6 kV and 25 kV.

Mo Grid 6kV			Mo Grid 25kV		
Element	Wt %	At %	Element	Wt %	At %
Mo	97.8 (97.3)	88.1 (86.7)	Mo	94.8	76.3
O	2.2 (2.2)	11.9 (11.6)	O	4.4	21.3
Al	(0.5)	(1.7)	Al	0.8	2.4
Mo Grid 6kV with "C"			Mo Grid 25kV with "C"		
Element	Wt %	At %	Element	Wt %	At %
Mo	94.6 (94.1)	70.7 (69.8)	Mo	87.2	48.8
C	3.3 (3.3)	19.9 (19.7)	C	8.2	36.5
O	2.1 (2.1)	9.4 (9.2)	O	3.9	13.2
Al	(0.5)	(1.3)	Al	0.7	1.4

Because of the complication of the large 0.18 keV peak in the Mo spectrum, EDS spectra (red solid spectra) obtained for the DC flake samples were often compared to the EDS spectra of the Mo grid obtained at the same accelerating voltage (overlaid as a black line spectra), and if the 0.18 keV peak appeared unchanged, then C was not identified as an element for quantitative computation. Only when a change in the size or position of the C peak was observed was the percentage of C computed. In that case, it is important to pay attention to the quantity of C as compared to the amount of C identified in the Mo grid or the Mo standard (as opposed to absolute values).

3. FESEM and EDS of DC Flakes

A total of 30 DC flakes were examined using the FESEM with corresponding EDS analysis. The flakes had various surface morphologies that could be described as one of the following: rough (high surface area porous texture), coated rough (appears to have a thin coating covering a rough porous substrate), rough directional (appears to have a thick coating deposited from a particular direction), coated nodules (appears as smooth little mounds) and smooth directional (appears to have a coated surface deposited from a particular direction). Examples of these surface textures are provided in Figures 15 to 19 with corresponding surface chemistry. Figure 15a provides an example of a rough surface (Flake B1 P4). The corresponding EDS spectrum obtained at 6 kV is provided in Figure 15b. This surface is comprised primarily of C (71.0 AT%) with O (17.5 AT%) and 5.5 AT% iron (Fe). There is less than 1 AT% of Al, Ta and Mo.
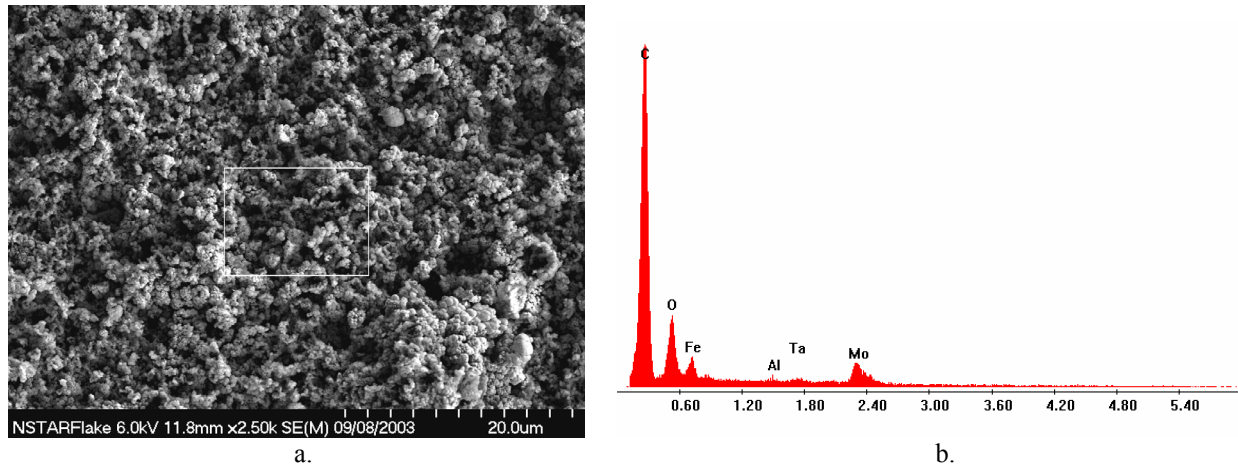

a.
b.

Figure 15. Flake B1 P4 with a rough surface morphology: a). Electron micrograph image of Flake B1 P4, and b). Corresponding EDS spectrum (9-8-03 S10) obtained from the box in the center of B1 P4.

Figure 16a shows an example of a coated rough surface. The corresponding EDS spectrum for this flake (B1 P6) obtained at 6 kV (obtained at the box shown in Figure 16a) is provided in Figure 16b along with the spectrum for a Mo Grid, shown as a black line spectrum. If the quantities are computed without identifying C, the surface is found

to be comprised primarily of Mo (63.9 AT%) with O (30.1 AT%), Fe (3.2 AT%) and Ta (2.9 AT %). If the semi-quantitative analysis is computed with C (a very small C peak is observed) then the data indicates that there is less Mo (51.0 AT%) with 20.5 AT% C, along with O (23.7 AT%), Fe (2.5 AT%) and Ta (2.3 AT%). Comparing 20.5 AT% C to 19.9 AT% computed for the grid when C is identified, implies there is no substantial amount of C on the surface of this flake. This sample shows the complication of identifying the C percentage when Mo is a predominant component, and the need to compare to the Mo grid data for identifying C quantities.
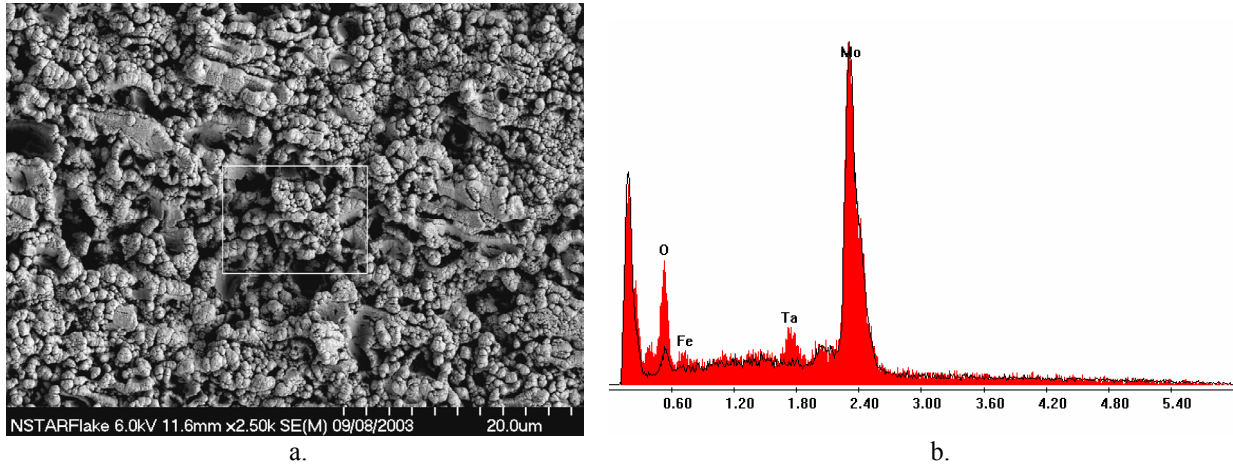

a.　　　　　　　　　　　　　　　　　　　　b.

Figure 16. Flake with a coated rough surface morphology: a). Electron micrograph image of Flake B1 P6, and b). Corresponding EDS spectrum (9-8-03 S12) obtained from the box area of Flake B1 P6 graphed along with the Mo grid spectrum.

Figure 17a provides an example of a rough directional surface texture, as found on the surface of flake B1 P2. Figure 17b shows the corresponding EDS spectrum obtained at 6 kV in the central region of Figure 17a. This spectrum is similar to that for the coated rough surface shown in Figure 16b, but has a more obvious C peak. This surface is comprised primarily of Mo (43.2 AT%) with C (32.0 AT%) and O (24.8 AT%). The solid colored spectrum for the flake has been graphed along with the 6 kV black line spectrum of the Mo grid sample. The difference in the amount of O is noticeable between these 2 spectra along with the presence of C and a small Ta peak in the DC flake spectrum. Again, for this spectrum, the amount of C would be less than computed due to the presence of the Mo line at 1.8 keV.
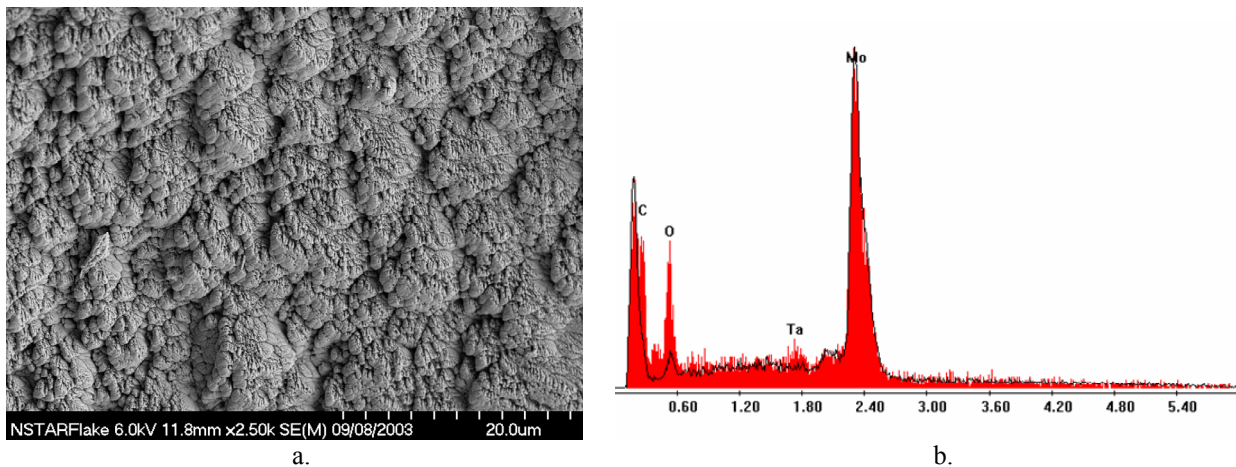

a.　　　　　　　　　　　　　　　　　　　　b.

Figure 17. Flake with a rough directional surface morphology: a). Electron micrograph image of Flake B1 P2, and b). Corresponding EDS spectrum (9-8-03 S8) obtained at the center of Flake B2 P6 graphed along with the Mo grid spectrum.

Figure 18a provides an example of a coated nodule surface texture, which look like smooth shallow mounds. Figure 18b shows the corresponding EDS spectrum obtained at 6 kV at the box location shown in Figure 18a. This surface is comprised primarily of Mo (34.7 AT%) with C (25.7 AT%), O (24.9 AT%) and Ta (14.7 AT%). The solid colored spectrum for the flake (B2 P1) has been graphed along with a black line spectrum of the Mo grid sample, also obtained at 6 kV. The difference in the amount of O is noticeable between these 2 spectra along with the presence of C and Ta in the DC flake spectrum. This flake provided the highest quantity of Ta observed.
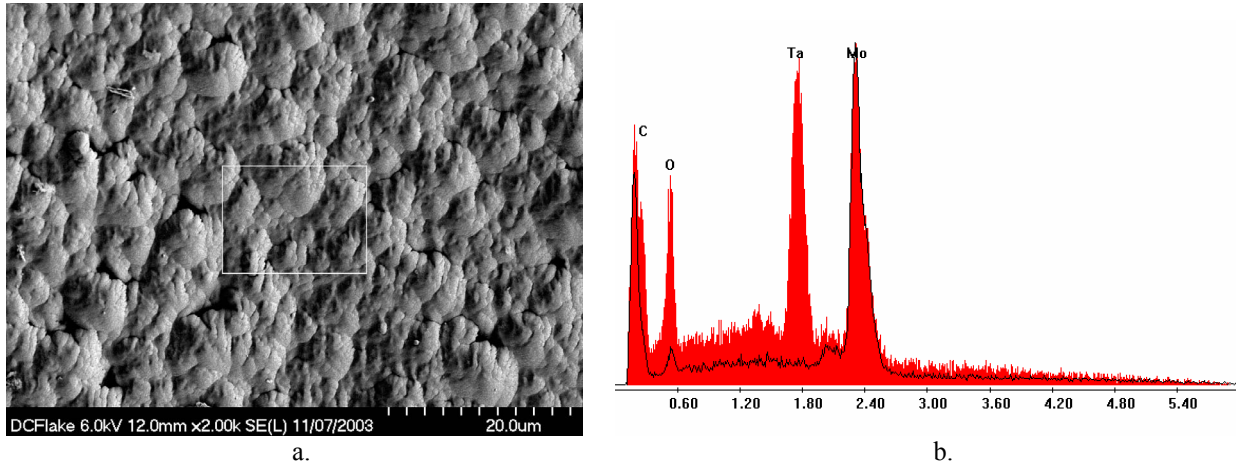

a.   b.

Figure 18. Flake with coated nodule surface morphology: a). Electron micrograph image of Flake B2 P1, and
b). Corresponding EDS spectrum (11-7-03 S2) obtained at the center of Flake B2 P1 graphed along with
the Mo grid spectrum.

Figure 19a provides an example of a smooth directional surface texture. Figure 19b shows the corresponding EDS spectrum obtained at 6 kV at the box location shown in Figure 19a. This surface is comprised of a high percentage of Mo (64.87 AT%) with O (31.6 AT%) and Ta (3.2 AT%). The solid colored spectrum for the flake (B2 P5) has been graphed along with the 6 kV black line spectrum of the Mo grid. The insert graph shows the solid colored spectrum for the smooth directional flake (B2 P5) graphed along with a black line spectrum from a Mo standard obtained at 6 kV. In this case the fit for both the 2.29 keV and 0.18 keV Mo peaks matches very well with the standard further confirming that C is not present in the surface of this flake.
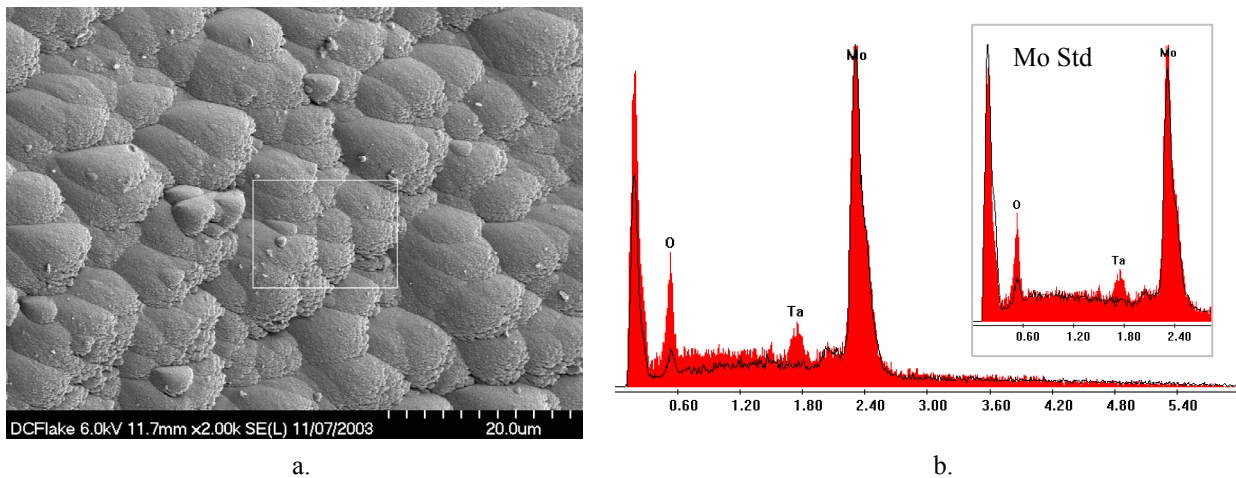

a.   b.

Figure 19. Flake with smooth directional surface morphology: a). Electron micrograph image of Flake B2 P5, and
b). Corresponding EDS spectrum (11-7-03 S5) obtained at the box area of B2 P5 graphed along with the
Mo grid spectrum. The B3 P5 spectrum graphed with the Mo standard spectrum is shown in the insert.

Examination of the edge of the flakes provided important information about the total make-up of the flakes. When examining the edges of the flakes, it was important to locate a broken edge to see if an inner layer or center layer exists. If a broken edge was not located, the flake could appear as a solid layer of Mo.

The majority of the flakes were found to be comprised of either two or three distinct layers. One flake (B2 P12) appeared to be comprised of a single layer of material. Edge and surface images of the single layer flake, which was rough and porous, and the corresponding chemistry is provided in Figures 20a to 20c, respectively. The surface, shown in 20b, is comprised of a high percentage of C (67.1 AT%) with O (19.7 AT%), Mo (6.0 AT%), Fe (5.0 AT%) and Ta (1.3 AT%). A small percent (0.9 AT%) of nickel (Ni) was also present.

It appears based on the chemistry of this single layer flake that it originated outside of the DC, likely the result of sputter erosion of the target with the resulting build-up of C on a downstream accelerator grid surface or hole wall, or the downstream face of the ground shield, that then (shortly before the end of the life test) spalled off the grid, falling into the vicinity of an accelerator hole where it was electro-statically attracted into the DC. Once such a flake lands within the DC it will gradually get coated with Mo, the primary element being deposited within the DC from ion grid erosion. Because the sputter containment mesh has a textured woven structure, the flakes arriving on the mesh could land flat and hence would be coated on one side with Mo, or the flake could land on edge (or at a titled edge) and be coated on both sides with Mo. Based on the chemistry of this single layer flake, it appears that this flake did not reside within the DC for a long period of time, because it has a small quantity (6.0 AT%) and does not have an obvious coating of Mo on either side of the C.
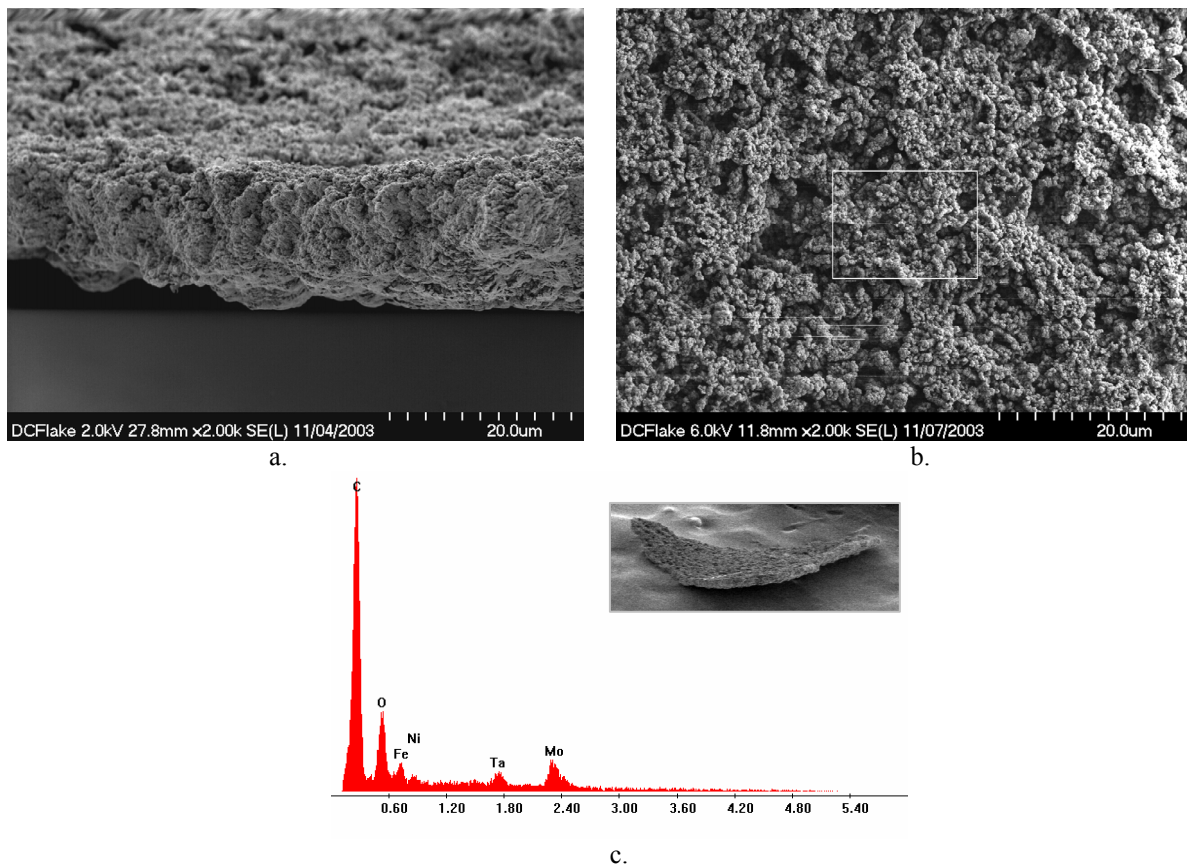

Figure 20. Single layer flake (B2 P12): a). Electron micrograph of the flake edge, b). Electron micrograph image of the flake surface, and c). Corresponding EDS spectrum (11-7-03 S4) obtained at the center of Flake B2 P12 shown in b).

Figure 21 provides an example of a two layered flake. Edge and surface images of the flake (B2 P3) are provided in Figures 21a and 21b, respectively. The edge view (shown in 21a) clearly shows two very distinct layers. The bottom layer is thicker than the top layer and is very rough and porous and looks a lot like the single layered Flake B2 P12. The top layer is much more solid in appearance and smooth. This layer appears to have a layered

structure to it, which would be consistent with stopping and re-starting of the thruster engine. The surface image shown in Figure 21b has been taken at a step-edge. Both the top smooth layer and the underlying bottom rough layer are visible in this image. The corresponding EDS spectrum for the rough thick bottom layer is provided in Figure 21c. It was obtained at the box location (S1) shown in Figure 21a. This thick rough layer is comprised primarily of C (83.2 AT%) with O (12.9 AT%) and Fe (3.8 AT%). The EDS spectrum for the smooth top layer is provided in Figure 21d. The flake spectrum is shown compared to the Mo grid spectrum in the figure insert. It was obtained at the upper right box location (S4) shown in Figure 21b. This smooth solid top layer is comprised of Mo (56.3 AT%) and O (43.7 AT%). This two layered flake can be characterized as a Mo-C flake. It is consistent with a C-rich downstream flake spalling off and arriving flat in the DC and residing long enough for a thick Mo layer to deposit on the exposed surface. The inserted electron microscope image shown in Figure 21c shows an area where the top Mo layer is wrapped down and partially around the edge. This provides a visible example of how the Mo can cover an underlying layer of C.
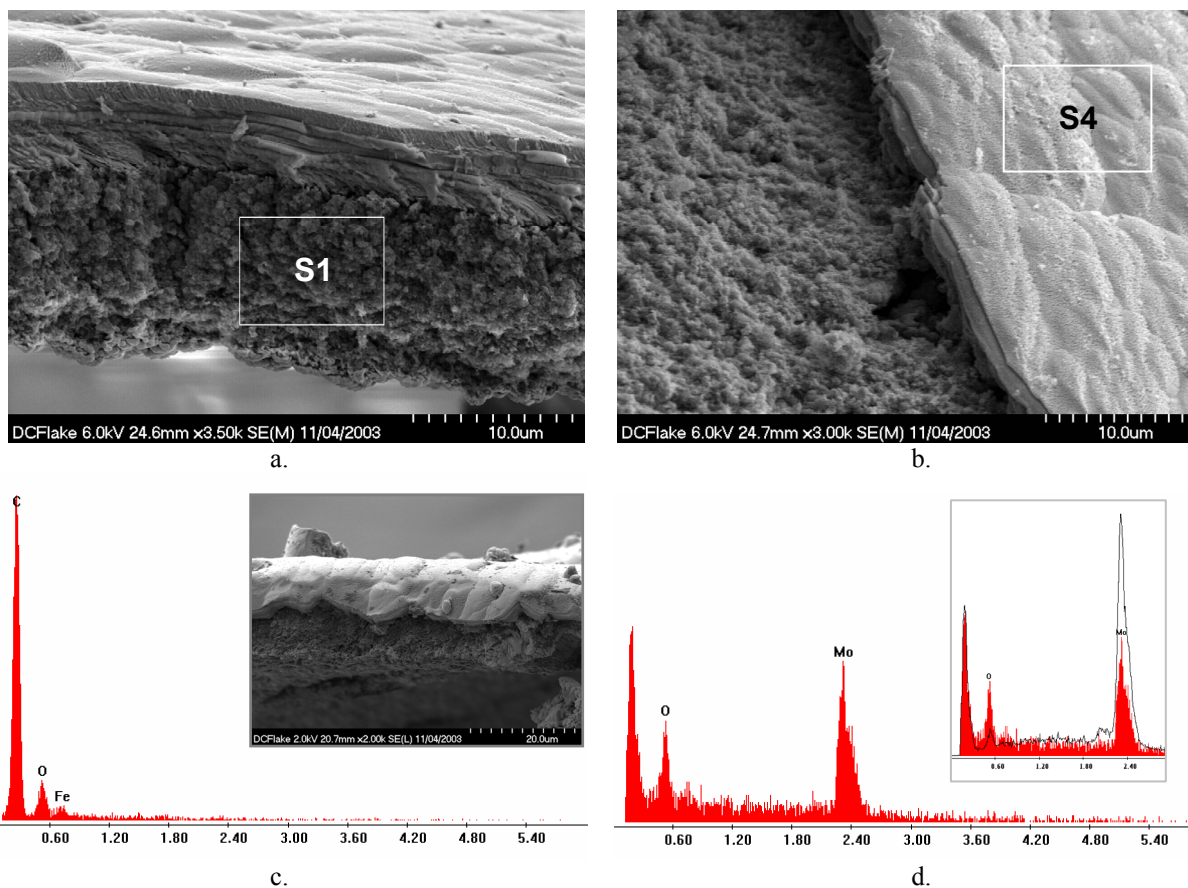

a.

b.

c.

d.

Figure 21. Two layered flake (B2 P3): a). Electron micrograph of the flake edge showing two distinct separate layers, b). Image of the flake surface at a step-edge, c). EDS spectrum (11-4-03 S1) of the rough layer obtained at the box shown in a), insert image shows a Mo surface coating wrapping around C base layer, and d). EDS spectrum (11-4-03 S4) of the smooth top layer obtained at the box shown in b).

Figure 22 provides an example of a three layered flake (B4 P1). This flake is 1.195 mm in length. A broken edge view of the flake is provided in Figure 22a and clearly shows three very distinct layers. The top layer in this image is a thin wavy layer. The center layer is a thick rough layer and the bottom layer is a rough nodular layer. The corresponding EDS spectra for these 3 layers are provided in Figure 22b to 22d, respectively. The EDS spectrum for the thin top layer is provided in Figure 22b and was obtained at the Box labeled S3 in Figure 22a. This layer is comprised of C (46.2 AT%), Mo (30.5 AT%), O (20.6 AT%) and Fe (2.7 AT%). The thick rough central layer is comprised primarily of C (79.1 AT%) with O (13.3 AT%) and Fe (5.3 AT%). There was less than 1 AT% of Al, Ta and Mo. The EDS spectrum was obtained at box S1 shown in Figure 22a. The EDS spectrum for the thick bottom layer is provided in Figure 22d and was obtained at box S2 in Figure 22a. This layer is comprised of

Mo (41.0 AT%), C (40.1 AT%), O (15.4 AT%), Fe (2.4 AT%) and Ta (1.1 AT%). An EDS spectrum was obtained on the surface of the thin top layer (3-23-04 S27), which indicated that this layer was comprised of Mo (66.2 AT%) with O (29.8 AT%) and Ta (4.0 AT%), with a very small C peak. The surface analysis performed on the flat section of the flake would provide more accurate EDS data than the spectrum obtained at S3. Therefore, this three layered flake can be characterized as a Mo-C-Mo flake. This flake is consistent with a C-rich downstream accelerator grid surface flake spalling off the grid and arriving in the DC on a tilted angle and residing long enough for Mo layers to deposit on both exposed surfaces.
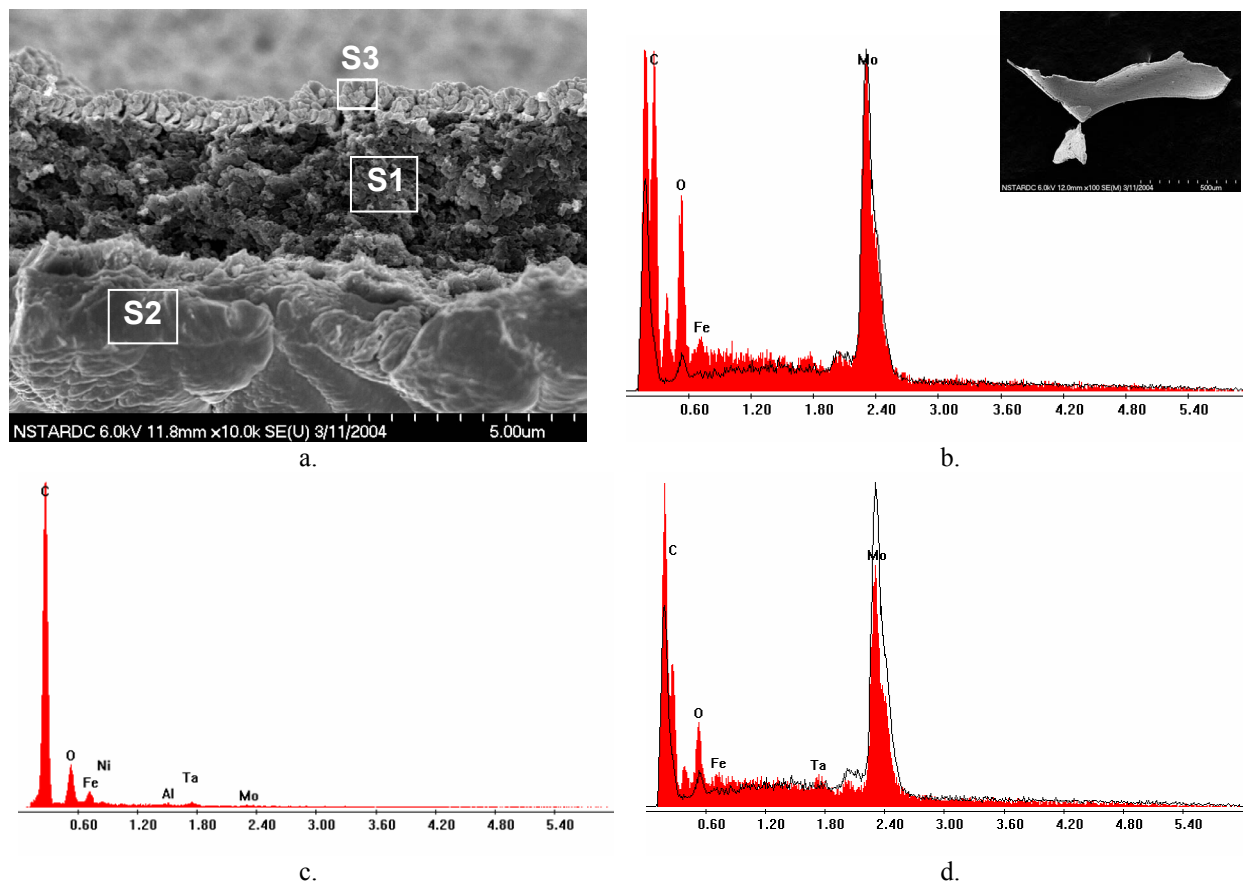

Figure 22. Three layered flake (B4 P1): a). Electron micrograph of the flake edge showing three distinct layers, b). EDS spectrum (3-11-04 S3) of the thin top layer obtained at the box shown in a), c). EDS spectrum (3-11-04 S1) of the rough center layer obtained at the box S1 shown in a) and d). EDS spectrum (3-11-04 S2) of the thick bottom layer obtained at the box S2 shown in a).

Figure 23 is an example of a dual-texture flake. Figure 23a shows an FESEM image of the flake with an optical microscope image as an insert for comparison. The optical image clearly shows a distinct difference between these regions in texture and hue. Figure 23b is a close-up electron image of the dual-texture region. This is also an example of a step-edge area. EDS spectra for the dark rough textured area and the light nodular textured area are provided in Figures 23c and 23d, respectively. The composition of the dark rough area (obtained at the box identified as S9) is comprised primarily of C (67.6 AT%) with O (16.4 AT%), Mo (12.7 AT%), Fe (2.4 AT%) and Ta (1.0 AT%). The composition of the light nodular area, which is metallic in appearance in the optical image, is comprised primarily of Mo (48.0 AT%), with C (28.1 AT%), O (18.7 AT%), Ta (3.5 AT%) and Al (1.6 AT%). The EDS spectrum was obtained from the box identified as S10 in Figure 23b. These results are consistent with the other flake data that show dark rough areas are comprised primarily of C, while the lighter metallic looking layers are comprised of a Mo-rich material. Again, these dual-texture flakes are consistent with a C-rich downstream flake spalling off and arriving in the DC and residing long enough for a Mo layer to deposit on the surface. The dual-texture appearance may be the result of a shadowing phenomenon. Shadowing could occur when two carbon-rich flakes land in the chamber with one overlapping the other in such a way that portions of the underlying flake are not

subject to Mo coating within the chamber. A dual-texture flake might also be the result of a 2 or 3 layered flake in which a portion of a Mo surface layer breaks off the flake during flake handling.
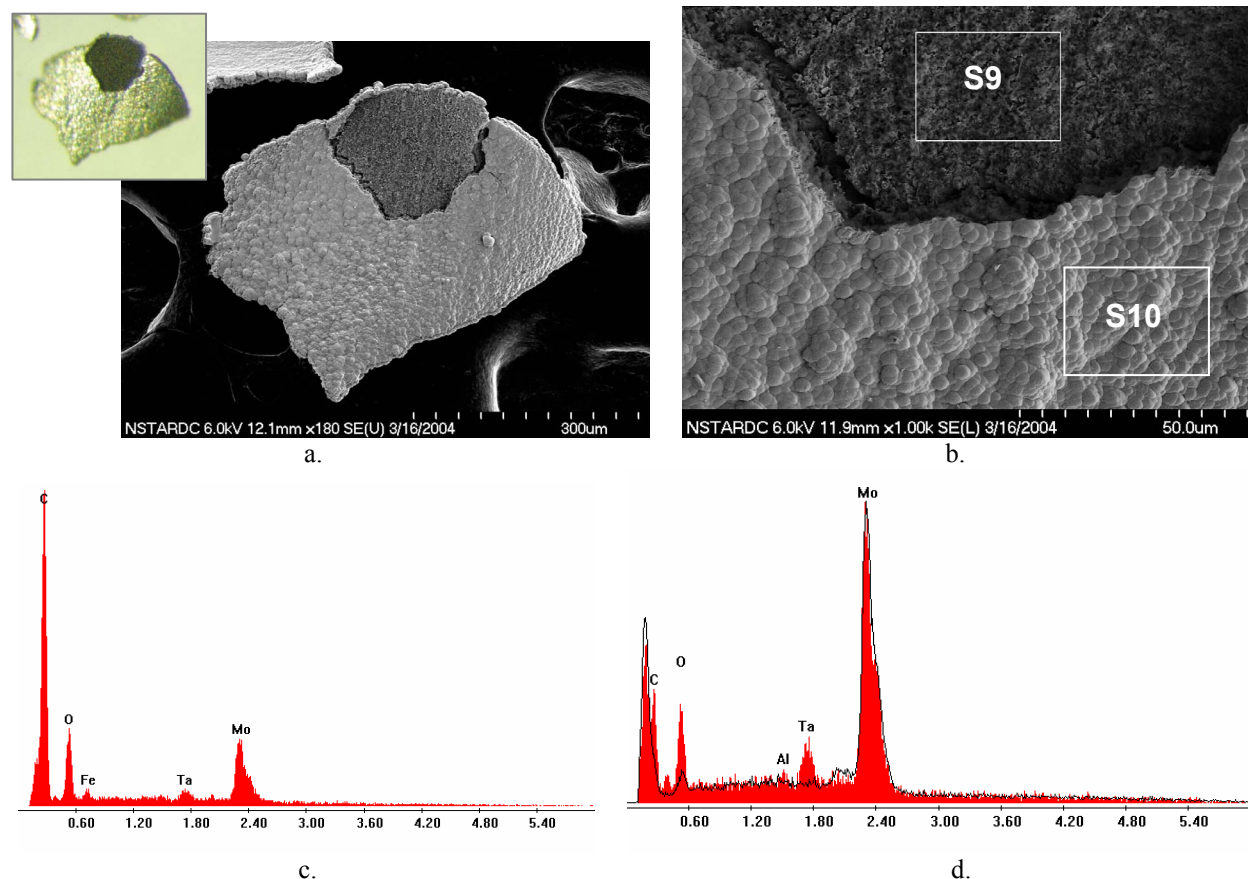

Figure 23. Dual-texture flake (B4 P5): a). Electron micrograph of the Flake B4 P5 showing two distinct textures, along with an optical microscope image insert, b). Electron micrograph showing a close-up of the dual-texture transition area, c). EDS spectrum (3-16-04 S9) of the dark rough layer obtained at box S9, and d). EDS spectrum (3-16-04 S10) of the nodular texture layer obtained at box S10.

Figure 24 is the largest DC flake analyzed with the electron microscope. This flake (B3 P1) was from the DC Flakes 3 container and is 1.556 mm in length. Figure 24a shows an FESEM image of the flake, while Figure 24b shows an image of a broken edge. Although the electron image does not clearly show it, this flake is a 3 layered flake. The EDS spectra for the 3 layers are provided in Figures 24c to 24f. The EDS spectrum of the top layer was collected at box S5 shown in the edge image and is comprised of Mo (36.7 AT%), C (32.0 AT%) and O (31.2 AT%). An EDS spectrum of this layer was also obtained as a surface scan (orientation as shown in Figure 24a) and is provided in Figure 24d. This spectrum indicates that there is a higher percentage of Mo (48.3 AT%) with less C (22.1 AT%) and O (21.4 AT%), and small amounts of Fe (4.2 AT%), Ta (2.6 AT%) and Al (1.4 AT%). The EDS spectrum for the center layer, indicated by S3 in the edge image, is provided in Figure 24e and indicated that it comprised of a high quantity of C (79.2 AT%) with O (14.7 AT%), Fe (4.2 AT%) and Mo (1.3 AT%). There was less than 1 AT% of Ni. The spectrum for the bottom layer, indicated by S4 in the edge image, is provided in Figure 24f and shows a highly oxidized surface with 39.9 AT% O along with Mo (32.8 AT%) and C (27.3 AT%). This large three layered flake can be characterized as a Mo-C-Mo flake. Again, having a central C-rich layer, this flake is consistent with the origin being the build-up of C on a downstream surface.
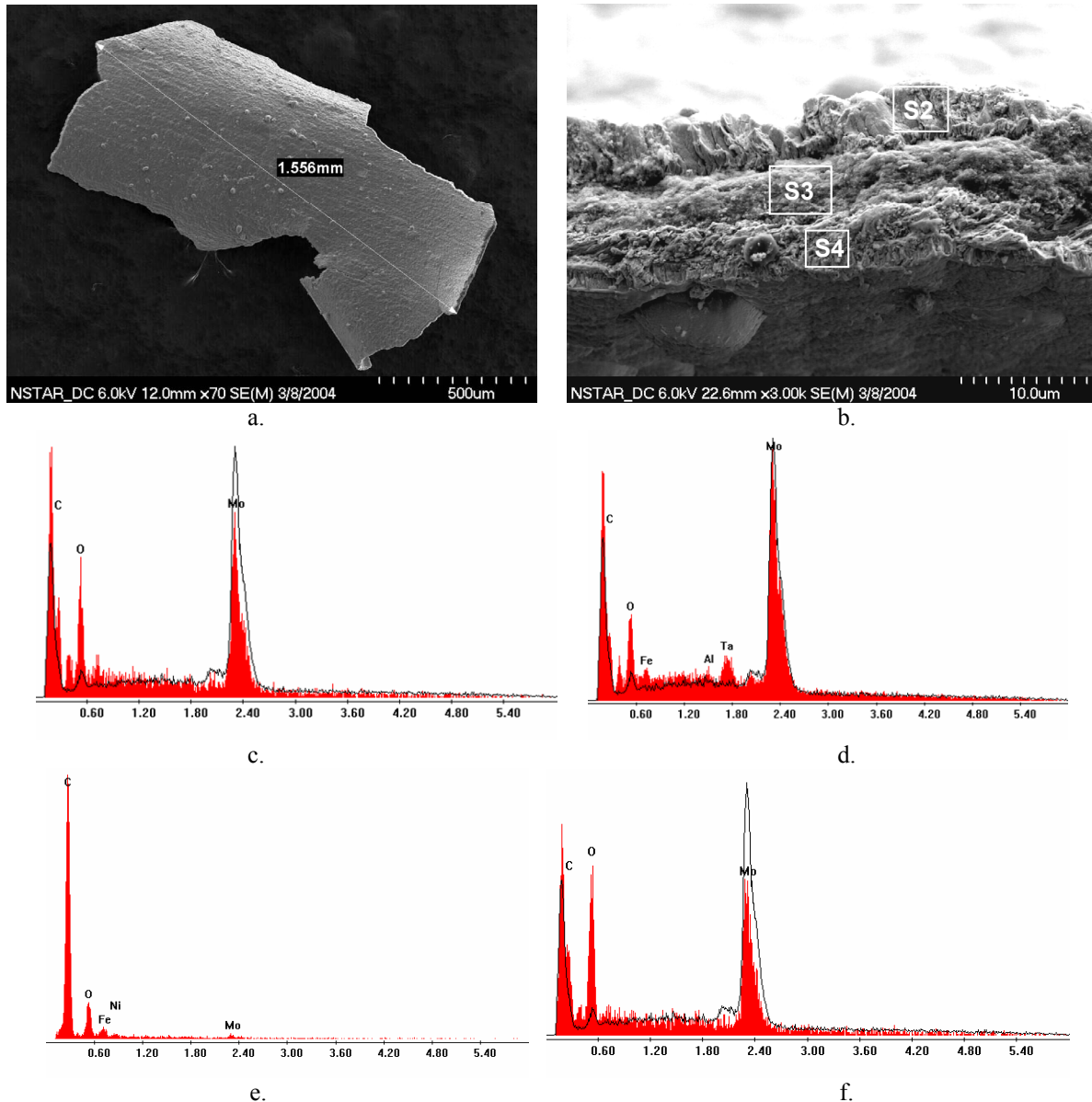
Figure 24. The largest analyzed DC flake (B3 P1): a). Electron micrograph of the flake, b). Electron micrograph showing a broken edge area, c). EDS spectrum (3-8-04 S5) of the top layer obtained at box S5, d). EDS spectrum (3-8-04 S1) of the surface of flake B3 P1 (top layer surface spectrum) shown along with a Mo grid spectrum (black line), e). EDS spectrum (3-8-04 S3) of the center layer obtained at box S3, and f). EDS spectrum (3-8-04 S4) of the bottom layer obtained at box S4.

Table 3 provides a list of all flakes analyzed with the FESEM and corresponding EDS analysis. The numbers 1-3 in the Edge Description column correspond to the visually different layers (#1 would be the top layer as seen in the FESEM image). The number in the Edge Chemistry, and in the Edge Thickness (where available) columns correspond to the layer identified in the Edge Description column. A total of 30 flakes were examined. Of those flakes, 27 had at least one C-rich layer. The three flakes that were not identified has having a C-rich layer did not have a broken edge visible. Therefore, it is very likely that a C-layer is present underneath the Mo surface coating, similar to the other flakes.   The longest dimension of the majority of these flakes is also provided in Table 3. These values are consistent with the histogram data. The thickness of the various layers has been determined when ever possible. If only one thickness value is provided, it is for the entire thickness of the flake (all layers). Based on the chemistry, multi-layer structure and size of the DC flakes it appears that these DC flakes originated from the downstream accelerator grid surface and hole walls and/or the downstream ground shield surface.

Table 3. DC Flakes Analyzed with FESEM and EDS.

Particle #	Length (mm)	Exposed Surface Morphology	# of Layers	Edge Description	Edge Chemistry at 6 kV (AT%)	Edge Thickness (µm)
B3 P1	1.556	Smooth directional	3	1. smooth 2. rough center 3. smooth	1. Mo (36.7), C (32.0)**, O (21.2) 2. C (79.2), O, (14.7), Fe (4.2), Mo (1.3) 3. O (39.9), Mo (32,8), C (27.3)**	14.1 ± 0.3
B2 P7	1.280	Smooth directional	3	1. smooth 2. rough center 3. smooth	1. Mo (BSE) 2. C (BSE) 3. Mo (BSE)	
B4 P2	1.249	Coated nodular (hole wall shape)	3	1. coated rough 2. rough center 3. coated rough	1. Mo appearance 2. C (76.8), O (13.7), Fe (5.7), Mo (1.3) 3. Looks like Mo	
B4 P1	1.195	Smooth directional	3	1. smooth thin 2. rough center 3. thick smooth	1. Mo (66.2), O (29.8), Ta (4.0) 2. C (79.1), O (13.3), Fe (5.3) 3. Mo (41.0), C (40.1), O (15.4), Fe (2.4)	1. 2.6 ± 0.3 2. 9.9 ± 1.0 3. 5.8 ± 0.3 total: 16.6 ± 1.3
B2 P10	1.189	Smooth		coated edge	C (40.7), Mo (31.1), O (21.1), Ta (6.1)	7.7 ± 0.5
B4 P11	1.126	Uniquely smooth	3	1. very thin solid 2. solid smooth center 3. very thin solid	1. Mo (50.8), C (34.8)**, O (10.7), Ta (3.7) 2. C (81.4), Fe (11.4), O (5.8), Ni (1.4) 3. Mo (45.1), C (43.3)**, O (7.9), Ta (3.7)	1. 1.3 ± 0.2 2. 5.8 ± 0.4 3. 0.9 ± 0.2 total: 7.9 ±- 0.8
B2 P1	1.023	Coated nodular	3	1. coated nodular 2. rough center 3. thin smooth coated	1. Mo (34.7), C (25.7), O (24.9), Ta (14.7) 2. C (81.6), O (12.5), Fe (3.3) Ta (1.1) 3. Mo (50.3), O (46.0), Ta (3.8)	13.2 ± 0.4
B4 P9	1.004	Coated nodular	2 or 3	1. smooth coating 2. rough center	1. Mo (47.2), C (31.2)**, O (11.9), Ta (9.7) 2. C (66.1), O (15.2), Mo (14.9), Fe (2.2), Ta (1.1)	
B2 P9	0.992	Coated nodular		edge not visible	C (45.9), Mo (30.3), O (21.4) - 25 kV	
B4 P4	0.995	Coated rough	3	1. thin coated rough 2. rough center 3. thick feather-like	1. O (51.2), Mo (43.0), Fe (5.0) 2. C primary peak identified - low counts 3. Mo appearance	
B4 P8	0.989	Coated nodular	3	1. smooth thick 2. rough center 3. coated nodular	1. Mo (45.9), C (36.1)**, O (17.4) 2. C (72.), O (15.6), Mo (8.8), Al (3.7) 3. Mo (40.5), C (34.7)**, O (23.3), Ta (1.6)	
B4 P3	0.966	Coated nodular		coated edge	C (39.4), Mo (35.7), O (21.8), Ta (3.4)	
B2 P3	0.893	Smooth directional	2	1. thick rough 2. smooth coated	1. Mo (56.3), O (43.7) & O (57.5), Mo (42.5) 2. C (83.2), O (12.9), Fe (3.8)	1. 5.0 ± 0.4 2. 12.3 ± 0.6 total: 17.4 ± 0.8
B1 P5		Coated rough	2	1. smooth coated 2. smooth coated	1. Mo (58.9), O (33.2), Fe (5.0), Ta (3.1) 2. C (40.8)**, Mo (36.7), O (20.9), Ta (1.6)	1. 6.4 ± 0.4 2. 7.8 ± 0.6 total: 14.1 ± 1.0+
B4 P10 broken	0.852	Smooth directional	3	1. smooth coating 2. rough center 3. smooth coating	1. Mo (39.3), C (36.5)*, O (21.0), Ta (3.2) 2. C (77.9), O (14.8), Fe (4.4) 3. Possibly Mo	
B2 P5	0.851	Smooth directional	3	1. smooth coated edge 2. step edge concave 3. surface convex	1. Mo (48.7), O (44.4), Fe (4.9), Ta (2.1) 2. C (73.1), O (15.0), Mo (6.7), Ta (2.7), Al (2.5) 3. Mo (64.8), O (32.), Ta (3.2)	18.9 ± 0.5
B2 P4	0.818	Rough	2	1. thick rough 2. very thin smooth	1. C (76.3), O (13.5), Fe (4.1), Ta (3.3) 2. C (43.3), Mo (30.3), O (24.8), Ta (1.6)	1. 10.0 ± 0.7 2. 3.3 ± 0.5 total: 13.2 ± 1.2
B2 P8	0.732	Smooth directional		edge not visible	Mo (53.4), C (23.7), O (19.5), Ta (3.4)	
B4 P6	0.721	Coated rough	3	1. rough coating 2. rough center 3. coated coating	1. Mo (78.3), O (26.5), C (25.8)**, Fe (1.9), Ta (1.8) 2. C (66.7), O (16.5), Mo (13.8), Fe (2.5) 3. Mo appearance	

Table 3 (Continued). DC Flakes Analyzed with FESEM and EDS.

Particle #	Length (mm)	Exposed Surface Morphology	# of Layers	Edge Description	Edge Chemistry at 6 kV (AT%)	Edge Thickness (µm)
B2 P2	0.729	Smooth directional	3	1. smooth coated 2. rough center 3. very thin smooth	1. Mo (70.0), O (6.7) 2. C (81.0), O (13.9), Fe (4.4) 3. Mo (46.1), C (42.6), O (3.5) (very thin layer)	1. 9.0 ± 0.5 2. 9.2 ± 1.2 3. 2.4 ±- 1.5 total: 20.6 ± 2.2
B2 P6	0.626	Coated rough		edge not visible	Mo, C, O, Ta	
B2 P11	0.566	Rough		edge not visible	Mo (41.5), O (35.5), C (20.1), Ta (2.9)	
B4 P7 2 flakes?	0.551	Rough coated 1/2 "scraped"	2	1. rough 2. feather-like	1. C (33.7)**, Mo (30.6), O (28.6), Ta (4.9), Fe (2.2)	
B4 P5	0.518	Coated nodular (shadowed particle)	3	1. smooth 2. rough center 3. smooth	1. Mo (48.0), C (28.1), O (18.7) Ta (3.5), Al (1.6) 2. C (67.6), O (16.4), Mo (12.7), Fe (2.4) 3. Looks like Mo	
B2 P12	0.445	Rough	1	1. rough	C (66.7), O (19.5), Mo (5.9), Fe (4.9), Ta (1.3)	14.4 ± 1.2
B1 P1		Coated rough	3	1. coated rough 2. rough center 3. feather-like	1. Mo (57.5), O (38.2), Ta (3.0), Al (1.3) (surface) 2. C (69.9), O (17.2), Fe (8.3), Ni (2.0), Al (1.5) 3. Mo (50.9), C (24.3)*, O (23.4), Ta (1.5)	1. 13.3 ± 1.1 2. 14.2 ± 0.4 3. 1.2 ± 0.2 total: 28.9 ± 1.7[+]
B1 P2		Rough directional	3	1. coated rough 2. rough center 3. smooth directional	1. Mo (43.2), C (32)**, O (24.8) 2. C (74.6), O (15.3), Mo (8.8) - 25 KV 3. Mo (78.1), O (18.5), Ta (3.4)	
B1 P7		Smooth directional	3	1. coated nodular 2. rough center 3. feather-like	1. Mo (47.4), O (47.8), Fe (2.3) Al, (1.2), Ta (1.2) 2. C (76.1), O (15.6), Fe (3.8), Mo (2.7) 3. Mo (66.2), O (31.0), Ta (1.6), Al (1.2)	
B1 P4		Rough	2 or 3		1. C (71.0), O (17.5), Fe (5.5), Mo (5.0) 2. C (63.8), O (17.7), Mo (14.4), Fe (2.9) Ta (1.2)	
B1 P6		Coated rough		edge not visible	Mo (51.0), O (23.7), C (20.5), Fe (2.5), Ta (2.3)	

* C peak only slightly enhanced, C presence questionable
** C peak is small but distinct
[+] flake at angle measurement may be high

B. Atomic Oxygen Exposure for Mass Loss Analysis

Atomic oxygen exposure was conducted to determine what percentage of the flakes was composed of C based on mass loss. This is because atomic oxygen will oxide organic components, such as C, with resulting volatile oxidation products. The initial mass measurements for the fused silica slide and the slide with the flake particles are provided in Table 4. The post atomic oxygen exposure measurements of the slide with the flakes, and the corresponding mass loss, in terms of percent loss, are provided in Table 5.

Table 4. Pre-Atomic Oxygen Exposure Mass Measurements.

Initial Mass of Clean Slide (mg)	Average (mg)	Initial Mass of Slide and Flakes (mg)	Average (mg)	Initial Mass of Flakes, M_T (mg)
0.850 0.850 0.850	0.850	2.638 2.634 2.633	2.635	1.785

Table 5. Post-Atomic Oxygen Exposure Mass Measurements.

Final Mass of Slide and Flakes (mg)	Average (mg)	Final Mass of Flakes, M_T' (mg)	Mass Loss (mg)	Percent Mass Loss (%)
2.226 2.225 2.224	2.225	1.375	0.410	23.0

The total mass of the flakes analyzed, M_T, is represented by the following equation

$$M_T = M_{Mo} + M_C = \rho_{Mo}AX_{Mo} + \rho_C AX_C \qquad (1)$$

where $M_T = 0.001785$ g, $\rho_{Mo} = 10.28$ g/cm^3 (density of Mo), $\rho_C = 2.26$ g/cm^3 (density of C), A is the total area of the measured flakes, X_C is the average thickness of the C layer in the flakes and X_{Mo} is the average thickness of the Mo layers in the flakes. After ashing for 115 hours, the mass of the ashed flakes, M_T', represents the total mass of the Mo originally contained in the flakes

$$M_T' = M_{Mo} = \rho_{Mo}AX_{Mo} \qquad (2)$$

where $M_T' = 0.001375$ g. Equations (1) and (2) combine to

$$M_T/M_T' = 1 + \rho_C X_C /\rho_{Mo}X_{Mo} \qquad (3)$$

solving (3) for X_C/X_{Mo} gives

$$X_C/X_{Mo} = \rho_{Mo}/\rho_C(M_T/M_T' - 1) \qquad (4)$$

solving (4) for X_{Mo} gives

$$X_{Mo} = X_C \rho_C/\rho_{Mo}(M_T'/M_T - M_T') \qquad (5)$$

but the average total flake thickness, X_T, prior to ashing is given by

$$X_T = X_C + X_{Mo} \qquad (6)$$

combining Equations (5) and (6) gives

$$X_T = X_C + X_C \rho_C/\rho_{Mo}(M_T'/M_T - M_T') \qquad (7)$$

solving Equation (7) for X_C gives

$$X_C = X_T/1 + \rho_C/\rho_{Mo}(M_T'/M_T - M_T') \qquad (8)$$

putting all of the known values into Equation (8) and assuming an average flake thickness of 17 μm (see average downstream accelerator grid thicknesses from section C below), X_C is determined to be 9.8 μm. Using this value in Equation (6), X_{Mo} is determined to be 7.2 μm. These average thickness values for C and Mo were used to estimate flake geometries.

The first example is a two layered flake, which would occur if a carbon flake landed flat in the chamber and was coated with Mo on one side only. This flake would have a ≈9.8 μm thick layer of C coated with ≈7.2 μm coating of Mo. The second example is a triple layered flake, the result of a C flake that landed vertically in the DC chamber and was coated with Mo on two sides. In this model, the thickness of the central C layer would be ≈9.8 μm and the two Mo layers ≈3.6 μm thick each. Figure 25 shows schematic drawings of these flake geometries based on the mass loss calculations. As stated before, these theoretical measurements are based on the average accelerator grid flake thickness. The length of time an individual flake was in the chamber would greatly influence the thickness of Mo coating on the C.

Based on DC flake edge thickness measurements, the flakes were found to vary in thickness from 7.7 to 28.9 μm, but were typically from 13.2 to 20.6 μm. For the flakes whose cross-section C layer was visible, it was found that the C layer varied from 7.8 to 12.3 μm thick. The average thickness for the C layer (10.1 μm) is consistent with the average C thickness (9.8 μm) computed based on mass loss. The C-based single layer flake had a thicker C layer at 14.4 μm.

3.6 μm   9.8 μm   3.6 μm
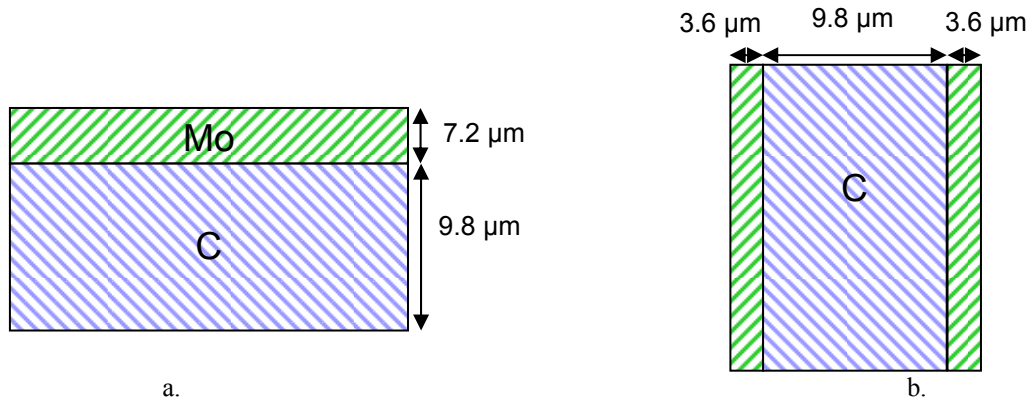
Mo   7.2 μm

C   9.8 μm

C

a.

b.

Figure 25. Schematic representation of the flake geometries based on mass loss calculations: a). Two layer flake geometry, and b). Three layer flake geometry.

C. Downstream Accelerator Grid Surface Flakes

An optical microscope image of one of the large downstream accelerator grid surface flakes is shown in Figure 26. The nonsymmetrical shape of the grid holes are reflected in this debris flake.
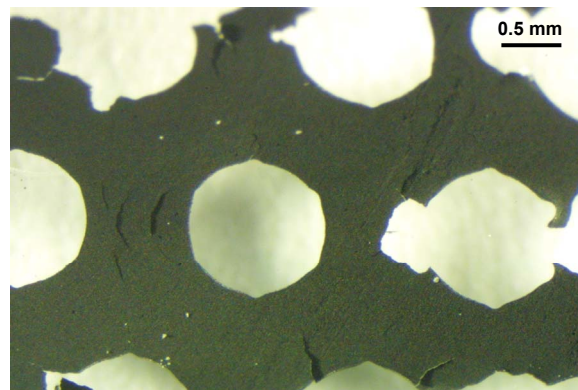

0.5 mm

Figure 26. Downstream accelerator grid surface flake.

The downstream accelerator grid flakes are black in appearance and the surfaces are very porous and rough, as shown in the FESEM image shown in Figure 27a. The corresponding EDS spectrum for the box area in the center of the image in 27a is provided in Figure 27b. As can be seen the downstream accelerator grid surface is composed primarily of C (75.0 AT%), and O (9.9 AT%), with stainless steel components (6.0 AT% Fe and 7.4 AT% chromium (Cr)) and less than 1 AT% of Ni, Al, and Ta. The Ta may be a result of thruster materials depositing on the facility walls, which was further ion sputtered and re-deposited back onto the accelerator grid.

The downstream accelerator grid flakes do not have distinct separate layers like the majority of the DC flakes, but appear as a single layer flake. Images of the edges of 2 different flakes are shown in Figure 28 along with thickness markers on 2 of the images. The edges have two types of appearances; they either look similar to the surface (very porous) or they appear to have a linear sheared fracture surface. Four particles were imaged and the thicknesses at 20 different edge locations were measured. The average thickness of the downstream accelerator grid flakes was found to be 16.9 μm. This is similar to the C-rich single layer DC flake (B2 P12) that was found to be 14.4 μm thick.
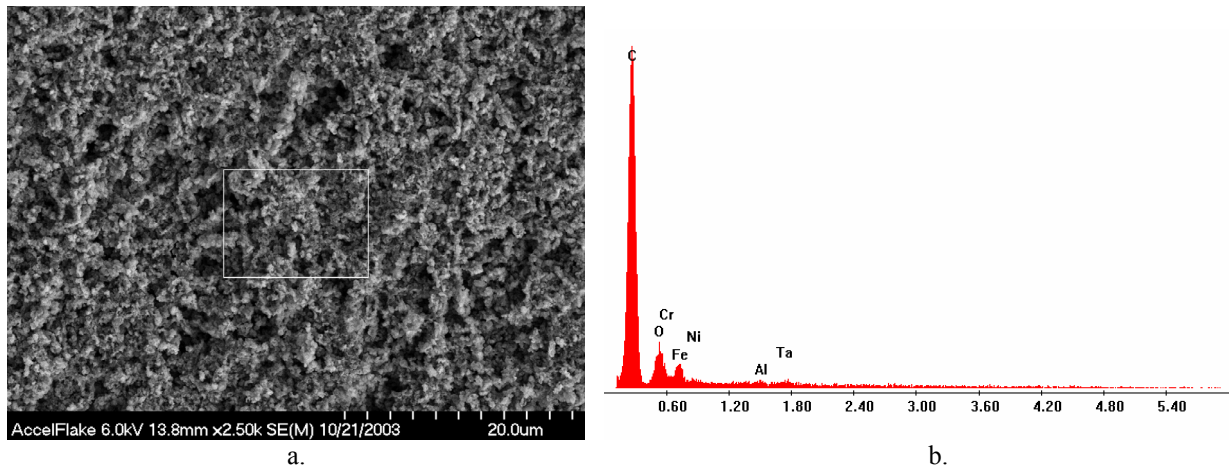
Figure 27. Downstream accelerator grid flake particle: a). Electron image of the surface of the flake, and b). Corresponding EDS spectrum (10-21-03 S2).
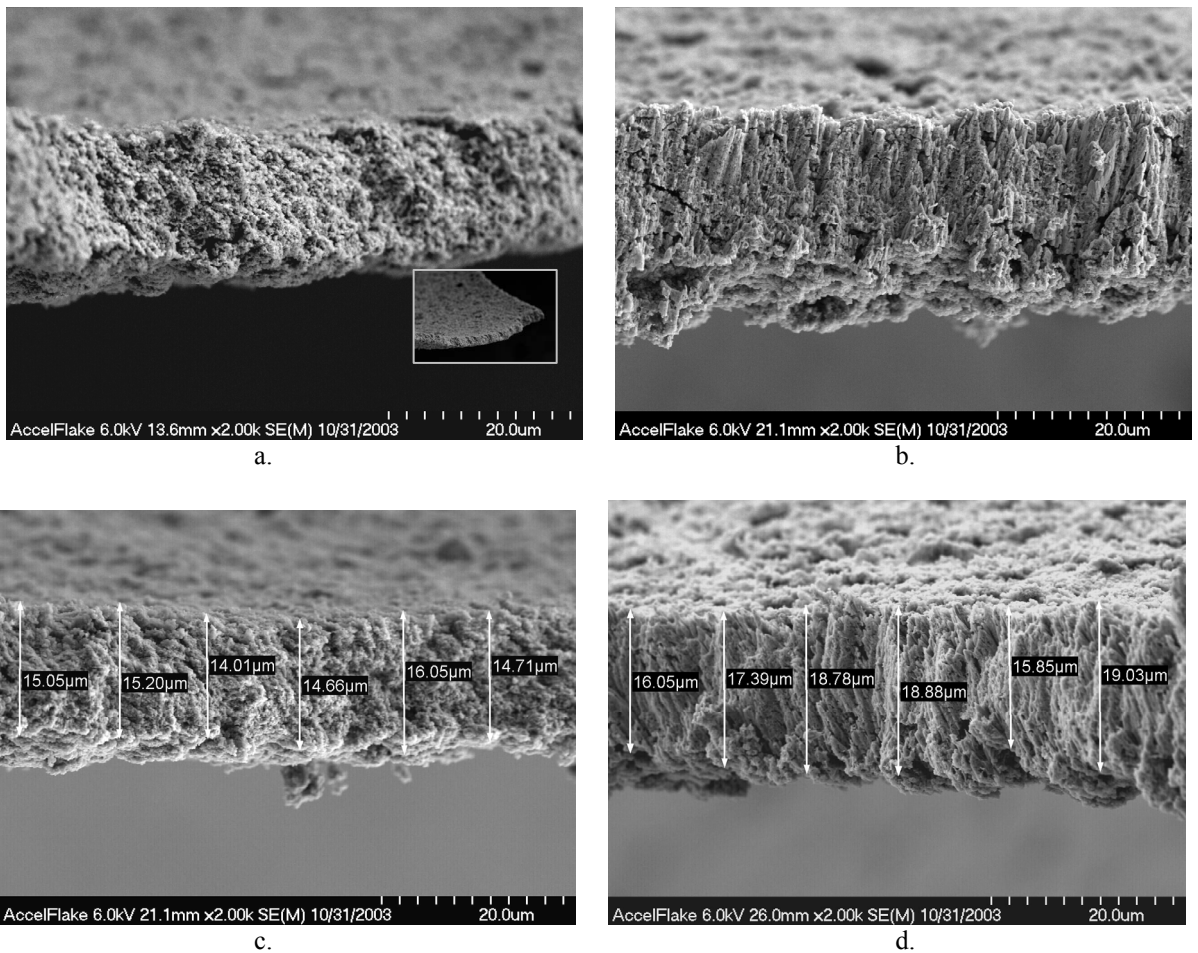

Figure 28. Edge morphologies for downstream accelerator grid flake particles: a). rough edge, b). sheared edge, c). rough edge with thickness measurements, and d). sheared edge with thickness measurements.

The chemistry of the edge of the downstream accelerator grid flakes appears to be very similar to the chemistry obtained on the surface (shown in Figure 27). Figure 29 shows the edge of a flake and the corresponding EDS spectrum that was obtained at the center of the film edge. As can be seen the downstream accelerator grid edge

surface was composed primarily of C (62.0 AT%), with O (8.5 AT % O), stainless steel components (11.7 AT% Fe, 13.5 AT% Cr, and 2.0 AT% Ni), Mo (1.2 AT%) and less than 1 AT% of Ta and Al. This edge area had less C and more stainless steel components than the surface provided in Figure 27a and also had a small amount of Mo (1.2 AT%).

a.   b.
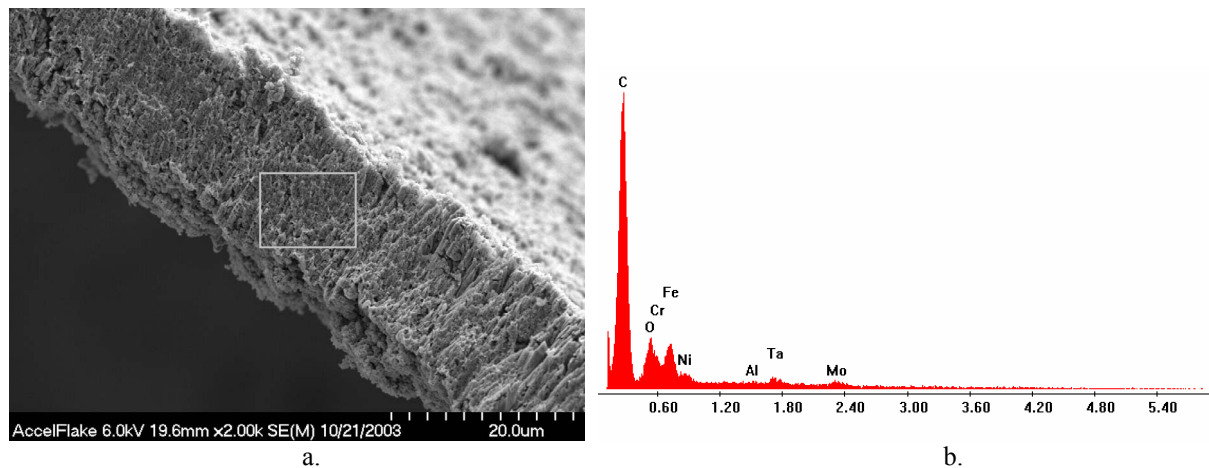
Figure 29. Edge morphology and corresponding chemistry of a downstream accelerator grid flake particle: a). Electron image of edge of flake, and b). Corresponding EDS spectrum (10-21-03 S3) obtained at the box shown in a).

Upon comparing the surface texture and corresponding chemistry of the downstream accelerator grid flakes to the DC flakes with a rough layer, very strong similarities exist. For example, if one compares the surface texture of a typical rough DC flake, as shown in Figure 15a, with that for the downstream accelerator flake shown in Figure 27a, the texture appears the same. Likewise, if one compared the EDS spectrum for the rough DC flake shown in Figure 15b with that for the downstream accelerator flake shown in Figure 27b, the spectra are very similar.   The primary difference is the presence of a small Mo and Ta peaks in the DC flake spectrum, which would have resulted from Mo and Ta deposition once the flake was inside the DC chamber. This comparison further supports the theory that the DC flakes originated from C deposition on downstream surfaces.

D. Sputter Containment Anode Mesh Samples

GRC analyzed samples of the thruster's containment mesh. As mentioned previously, the purpose of the analysis was to determine if the grit-blasted sputter containment mesh functioned properly in retaining the coating deposited on it during the length of the run rather than allowing it to spall off into the chamber, possibly being the source of the DC flakes. The FESEM images of the containment mesh clearly showed that there is a coating deposited on the surface of the containment mesh and that the thickness of this coating increases from the cathode to the grid optics. Figure 30 provides electron images of one of the axial sets of containment mesh samples obtained at the same magnification for comparison. The samples shown in Figure 30a to 30f include Samples 3, 4, 5, 30, 31, and 32, respectively.   Sample 3 was located in the conical area closest to the cathode. Sample 4 was located in the center of the conical area. Sample 5 was located in the conical area near the edge of the conical/cylindrical intersection region. Sample 30 was located in the cylindrical section near the conical/cylindrical intersection region. Sample 31 was located in the center of the cylindrical section, and Sample 32 was located in the cylindrical region closest to the grids. The coating on Sample 3 appears the thinnest and the coating on Sample 32 appears to be the thickest.

The chemistry of the coating on the anode mesh was determined at GRC by EDS to be mostly Mo with small amounts of the components of stainless steel (Fe, Cr, Ni). No spalling is evident, even from the samples of containment mesh cut from the region closest to the optics, which had the thickest coating of all the regions. One set of mesh samples (Samples 21-26) were purposely scratched in an effort to induce spalling, even after being physically scraped the coating on the anode mesh samples did not show signs of spalling or lifting off. This provides evidence that the DC flakes did not originate from spalling of the containment mesh coating.
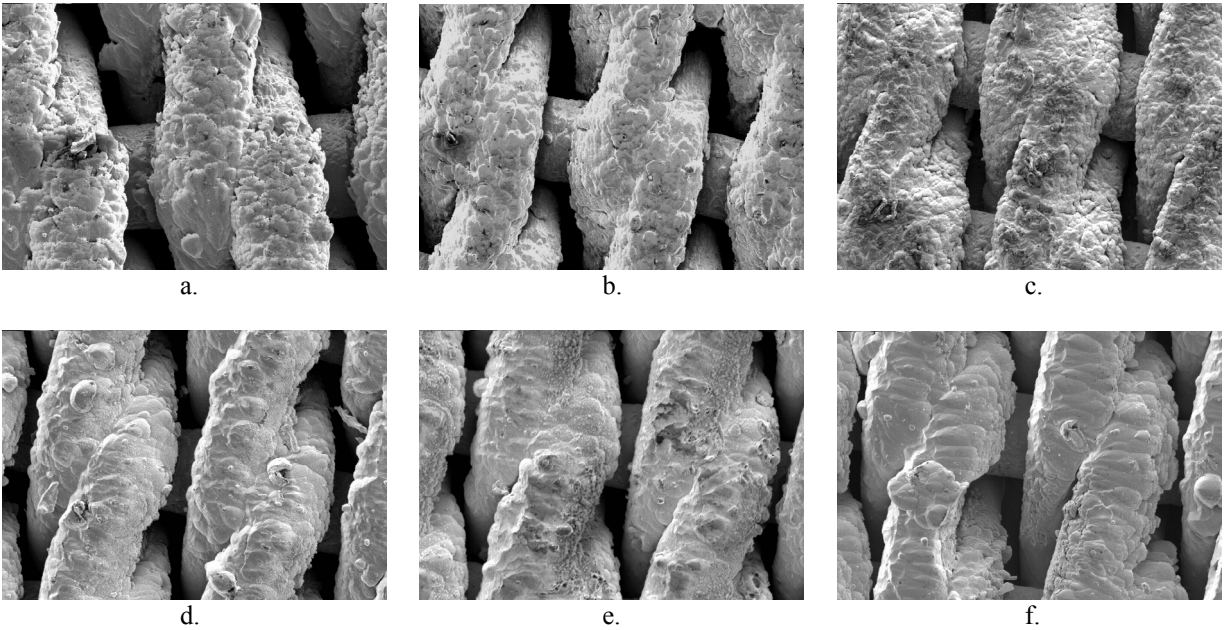
Figure 30. Anode mesh samples section in a radially similar position from within the DC: a). Sample 3, located in the conical region closest to the cathode, b) Sample 4, c). Sample 5, d). Sample 30, e). Sample 31 and f). Sample 32, located in the cylindrical region closest to the grids.

Two of the samples (Sample 21 and Sample 26) were sent to the University of Dayton Research Institute for additional analytical analysis. The mesh samples were cross-sectioned and potted, and the chemistry of the coating was determined using EDS. Figures 31a and 31b provide electron images of cross-sectioned Sample 21 and 26, respectively (Sample 21 was imaged at 1.5X higher magnification than Sample 26). The coating on Sample 21, which was closest to the cathode, was much thinner than on Sample 26 (closest to the grids) and it was found to be comprised of 65.0 AT% C, 14.8 AT% Mo, 10.9 AT% O, 3.3 AT% Fe, 2.6 AT% Xe, and 1.6 AT% Si (Si and Ta reside at the same peak location). The coating on Sample 26 was found to be thick and was comprised of 49.3 AT% C, 40.1 AT% Mo, 10.0 AT% O and 0.7 AT% Ta. It should be noted that these EDS data were obtained at 20 kV, which can excite Xe, whereas 6 kV does not.
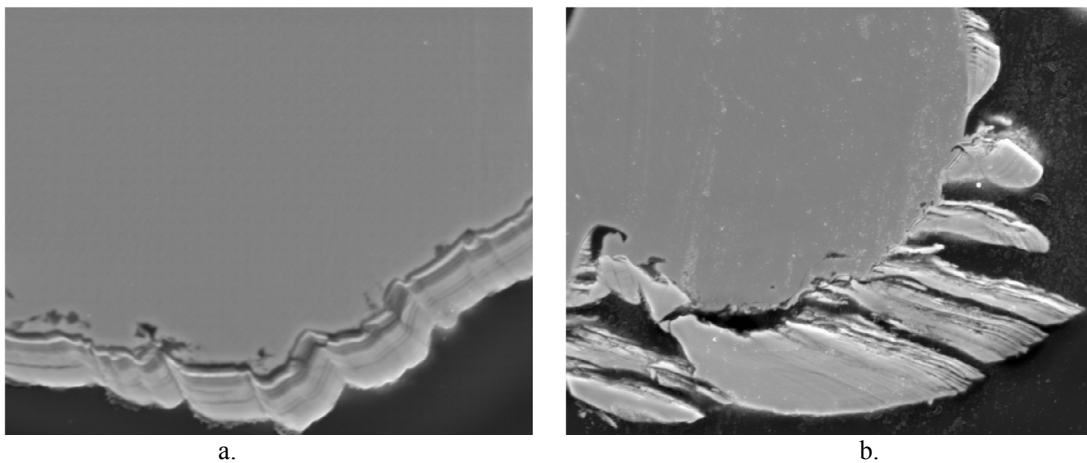

Figure 31. Electron microscope images of cross-sectioned anode mesh samples: a). Sample 21 located closest to the cathode, and b). Sample 26 located closest to the screen grid.

Extensive analyses of the mesh containment samples including mesh sample cross-sectioning and chemical analyses of individual layers seen through cross-sectioning have been conducted at JPL. Details of these analyses are reported by Garner in reference 9.

As another verification to show that the DC flakes did not originate from the containment mesh, electron images of several larger DC flakes have been compared with the anode mesh texture at approximately the same magnification, as shown in Figure 32. As can be seen by comparing these images, the DC flake particles do not replicate the woven texture of the anode mesh. The flakes are comparatively much smoother than the anode mesh texture and appear to have spalled off of a flat or curved smooth surface. Another comparison can be made between the anode mesh image and the largest DC flake (B3 P1) shown in Figure 24a.
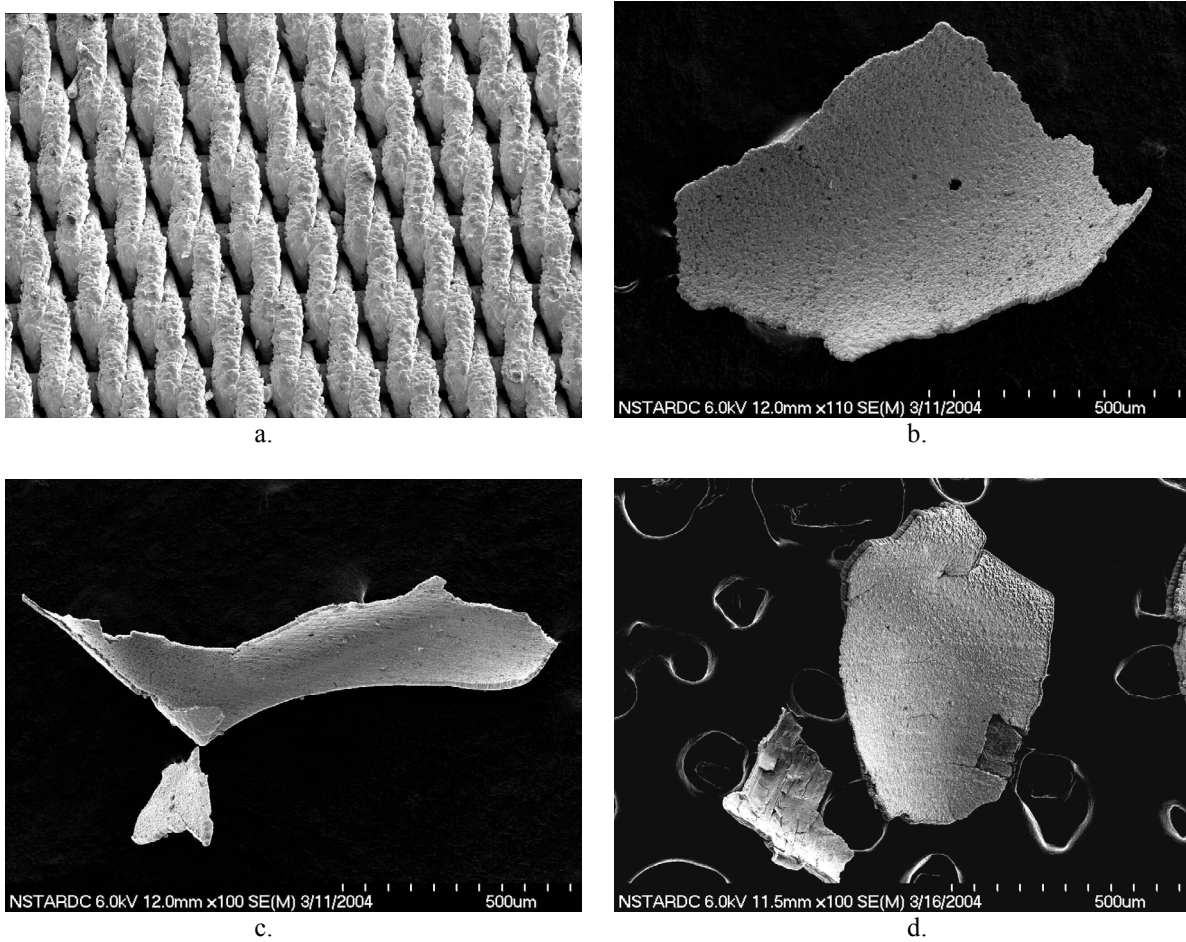

a.

b.

c.

d.

Figure 32. Comparison of the macro texture of the coated sputter containment mesh and DC flakes: a). Sputter containment mesh (Sample 21), b). DC Flake B4 P3, c). DC Flake B4 P1, and d). Flake B2 P6.

IV. Discussion

The origins of the flakes could be from 7 different potential locations as indicated in Table 6, and highlighted in Figure 5. The surface morphology and shape of the potential sources gives good indications of the morphology and shape of the resulting flakes that one would expect upon observation of those found in the DC. The maximum size of the flakes generated downstream of each of the grids would not be observed within the DC because the grids prevent the entry of flakes larger than the aperture diameters (except for a few that may enter the grid apertures end-on). If one compares the compositions possible for flakes from the various sources, their potential sizes, shapes and morphologies and the grid hole diameters, one is lead to believe that the flakes have all originated from facility sputter deposited C materials as opposed to internal thruster erosion. The flakes originate predominantly from

spalling of facility deposited coatings on the downstream face and hole walls of the accelerator grid, and from the downstream face of the ground shield. The production of the downstream carbon flakes, and hence the potential problems associated with the flake particles in the ELT ion thruster engine is a ground test artifact. Therefore, this problem would not occur in the space environment.

Table 6. Potential Origin Locations for DC Flakes.

Origin Number	Origin Location for Spalled Flakes	Surface Morphology and Shape	Composition Major (Minor)
1	Cathode keeper area	Smooth nearly flat	Ta (W, Mo, C)
2	Anode mesh	Rough curved	Mo (C, Ta, W)
3	Perimeter of upstream screen grid face	Smooth flat	Mo (C, Ta, W)
4	Screen grid hole wall	Smooth curved	Layered: Mo (C, Ta, W) on C (Mo) on Mo (C, Ta, W) or C (Mo) on Mo (C, Ta, W)
5	Accelerator grid hole wall	Smooth curved	Layered: Mo (C, Ta, W) on C (Mo) on Mo (C, Ta, W) or C (Mo) on Mo (C, Ta, W)
6	Perimeter of downstream accelerator grid face	Smooth nearly flat	C (Mo)
7	Downstream face of thruster ground shield	Smooth nearly flat	C (Mo)

V.   Summary and Conclusions

Upon post-test inspection of the NSTAR ELT DC numerous unexpected flakes were found on the floor of the DC. A particle size histogram based on measurements of ≈1500 flakes indicated that 10% of the flakes would be large enough to bridge the gap between the screen and accelerator grids based on the post-test grid gap distances. These flakes therefore have the potential for threatening the lifetime operation of the ELT engine, and their presence could be a threat to future ion engine performance and mission success. Therefore, extensive analyses were conducted to determine the origin of the flakes.

A total of 30 NSTAR ELT DC flakes were analyzed using FESEM and corresponding EDS semi-quantitative analysis. The analyses of the particles indicate that the majority of the DC flakes consist of a layered structure, typically with either 2 or 3 layers. The flakes comprising 2 layers were typically found to have a Mo-rich layer on one side and a C-rich layer on the other side. The flakes comprising 3 layers were found to be sandwich-like structures with Mo-rich exterior layers and a C-rich interior layer. The presence of the C rich layers indicates that these particles were produced by sputter deposition build-up on a surface external to the discharge chamber from ion sputter erosion of the C target in the test chamber. This contaminant layer became thick enough that particles spalled off, and then were electro-statically attracted into the ion thruster interior, where they were coated with Mo from internal sputter erosion of the screen grid and cathode components. Atomic oxygen tests provided evidence that the majority of the DC chamber flakes are composed of a significant fraction of C. Particle size histograms further indicated that the source of the particles was spalling of carbon flakes from the downstream accelerator grid

surface, downstream accelerator grid hole walls, or the downstream face of the ground shield, based on flake size. Analyses of flakes taken from the downstream surface of the accelerator grid were very similar in texture and chemistry as the C-rich layer of the DC flakes, providing additional supportive information. Furthermore, analyses of containment mesh samples combined with DC flake morphology and chemistry provide no evidence that the loose DC chamber flakes were generated from spalling of containment mesh deposited Mo. Therefore, the production of the downstream carbon flakes, and hence the potential problems associated with the flake particles in the NSTAR ELT ion thruster engine has been determined to be a facility induced effect and would not occur in the space environment.

References

[1]Brophy, J.R., "NASA's Deep Space 1 Ion Engine (Plenary)," Rev. Sci. Instrum., Vol. 73, No. 2., February 2002, pp.1071–1078.

[2]Sengupta, A., Brophy, J.R., Goodfellow, K.D., "Status of the Extended Life Test of the Deep Space 1 Flight Spare Ion Engine after 30,352 Hours of Operation," 39th AIAA/ASME/SAE/ASEE Joint Propulsion Conference and Exhibit, Huntsville, Alabama, July 2003, AIAA–2003–4558.

[3]Polk, J.E. et al., "Demonstration of the NSTAR Ion Propulsion System on the Deep Space One Mission," 27th International Electric Propulsion Conference, October 2001.

[4]Polk, J.E. et al., "Validation of NSTAR Propulsion system on the DS1 Mission," AIAA–99–2246, June 1999.

[5]Polk, J.E. et al., "In-Flight Performance of the NSTAR Ion Propulsion System on the Deep Space One Mission," Z8_0304.pdf, IEEE Aerospace Conference Proceedings, March 2000.

[6]Sengupta, A., Brophy, J.R., Garner, C.E., and Anderson, J.A., "An Overview of the Results from the 30,000 Hour Life Test of the Deep Space One Flight Spare Ion Engine," 52nd JANNAF Propulsion Meeting, Las Vegas, NV, May 2004.

[7]Sengupta, A., Brophy, J., Anderson, J., Garner, C., Banks, B., de Groh, K., and Karniotis, C., "An Overview of the Results from the 30,000 Hr Life Test of Deep Space 1 Flight Spare Ion Engine," 40th AIAA/ASME/SAE/ASEE Joint Propulsion Conference and Exhibit, Fort Lauderdale, FL, July 2004, AIAA–2004–3608.

[8]Sengupta, A., Anderson, J.R., Brophy, J.R., Rawlin, V.K., and Sovey, J.S., "Performance Characteristics of the Deep Space 1 Flight Spare Ion Thruster Long Duration Test after 21,300 Hours of Operation," 38th AIAA/ASME/SAE/ASEE Joint Propulsion Conference and Exhibit, Indianapolis, Indiana, July 2002, AIAA–2002–3959.

[9]Garner, C., Sengupta A., and Kulleck, J., "An Evaluation of the Discharge Chamber of the 30,000 Hr Life Test of the Deep Space 1 Flight Spare Ion Engine," 40th AIAA/ASME/SAE/ASEE Joint Propulsion Conference and Exhibit, Fort Lauderdale, FL, July 2004, AIAA–2004–3609.

[10]Anderson, J., Sengupta A., and Brophy, J., "Post- Test Analysis of the Deep Space 1 Spare Flight Thruster Ion Optics," 40th AIAA/ASME/SAE/ASEE Joint Propulsion Conference and Exhibit, Fort Lauderdale, FL, July 2004, AIAA–2004–3610.

REPORT DOCUMENTATION PAGE

1. AGENCY USE ONLY (*Leave blank*)	2. REPORT DATE March 2005	3. REPORT TYPE AND DATES COVERED Technical Memorandum

4. TITLE AND SUBTITLE

NSTAR Extended Life Test Discharge Chamber Flake Analyses

5. FUNDING NUMBERS

WBS–22–319–20–E1

6. AUTHOR(S)

Kim K. de Groh, Bruce A. Banks, and Christina A. Karniotis

7. PERFORMING ORGANIZATION NAME(S) AND ADDRESS(ES)

National Aeronautics and Space Administration
John H. Glenn Research Center at Lewis Field
Cleveland, Ohio 44135–3191

8. PERFORMING ORGANIZATION REPORT NUMBER

E–14694

9. SPONSORING/MONITORING AGENCY NAME(S) AND ADDRESS(ES)

National Aeronautics and Space Administration
Washington, DC 20546–0001

10. SPONSORING/MONITORING AGENCY REPORT NUMBER

NASA TM—2005-213195
AIAA–2004–3612

11. SUPPLEMENTARY NOTES

12a. DISTRIBUTION/AVAILABILITY STATEMENT

Unclassified - Unlimited
Subject Categories: 20, 18, 14, and 23   Distribution: Nonstandard

Available electronically at http://gltrs.grc.nasa.gov

This publication is available from the NASA Center for AeroSpace Information, 301–621–0390.

12b. DISTRIBUTION CODE

13. ABSTRACT *(Maximum 200 words)*

The Extended Life Test (ELT) of the NASA Solar Electric Propulsion Technology Readiness (NSTAR) ion thruster was concluded after 30,352 hours of operation. The ELT was conducted using the Deep Space 1 (DS1) back-up flight engine, a 30 cm diameter xenon ion thruster. Post-test inspection of the ELT engine revealed numerous contaminant flakes distributed over the bottom of the cylindrical section of the anode within the discharge chamber (DC). Extensive analyses were conducted to determine the source of the particles, which is critical to the understanding of degradation mechanisms of long life ion thruster operation. Analyses included: optical microscopy (OM) and particle length histograms, field emission scanning electron microscopy (FESEM) combined with energy dispersive spectroscopy (EDS), and atomic oxygen plasma exposure tests. Analyses of the particles indicate that the majority of the DC flakes consist of a layered structure, typically with either two or three layers. The flakes comprising two layers were typically found to have a molybdenum-rich (Mo-rich) layer on one side and a carbon-rich (C-rich) layer on the other side. The flakes comprising three layers were found to be sandwich-like structures with Mo-rich exterior layers and a C-rich interior layer. The presence of the C-rich layers indicates that these particles were produced by sputter deposition build-up on a surface external to the discharge chamber from ion sputter erosion of the graphite target in the test chamber. This contaminant layer became thick enough that particles spalled off, and then were electro-statically attracted into the ion thruster interior, where they were coated with Mo from internal sputter erosion of the screen grid and cathode components. Atomic oxygen tests provided evidence that the DC chamber flakes are composed of a significant fraction of carbon. Particle size histograms further indicated that the source of the particles was spalling of carbon flakes from downstream surfaces. Analyses of flakes taken from the downstream surface of the accelerator grid provided additional supportive information. The production of the downstream carbon flakes, and hence the potential problems associated with the flake particles in the ELT ion thruster engine is a facility induced effect and would not occur in the space environment.

14. SUBJECT TERMS

Electric propulsion; Ion thruster; Ion engine; Ion propulsion; Ion optics; Grid; NSTAR; Spacecraft; Erosion

15. NUMBER OF PAGES
34

16. PRICE CODE

17. SECURITY CLASSIFICATION OF REPORT Unclassified	18. SECURITY CLASSIFICATION OF THIS PAGE Unclassified	19. SECURITY CLASSIFICATION OF ABSTRACT Unclassified	20. LIMITATION OF ABSTRACT